İSTANBUL TECHNICAL UNIVERSITY ★ INSTITUTE OF SCIENCE AND TECHNOLOGY

NUMERICAL COMPUTATION OF TURBULENT FLOW IN COMPLEX GEOMETRIES

M.Sc. Thesis by

Barış ADİLOĞLU, B.Sc.

Department : Mechanical Engineering

Programme: Thermofluids

JUNE 2005

İSTANBUL TECHNICAL UNIVERSITY ★ INSTITUTE OF SCIENCE AND TECHNOLOGY

NUMERICAL COMPUTATION OF TURBULENT FLOW IN COMPLEX GEOMETRIES

M.Sc. Thesis by

Barış ADİLOĞLU, B.Sc.

(503031100)

Date of submission : 9 May 2005

Date of defence examination: 2 June 2005

Supervisor (Chairman): Asst. Prof. Dr. Levent KAVURMACIOĞLU

Members of the Examining Committee Prof. Dr. Seyhan ONBAŞIOĞLU (İTÜ.)

Assoc. Prof. Dr. Aydın MISIRLIOĞLU (İTÜ.)

JUNE 2005

ACKNOWLEDGEMENTS

First of all I want to give my special thanks to my supervisor Asst. Prof. Dr. Levent Kavurmacıoğlu, for all his support, valuable instructions and kindness towards me during my study.

Thanks to all my professors in İstanbul Technical University for every bit of information I have learned from them.

Last but not least, I want to thank my family for their morale support, encouragement and understanding all the time.

June, 2005 Barış Adiloğlu

TABLE OF CONTENTS

ABBREVIATIONS

CFD **:** Computational Fluid Dynamics
FVM : Finite Volume Method
PWIM : Pressure Weighted Interpolation Method
SIMPLE : Semi-Implicit Method for Pressure Linked Equations
SIMPLEC : Semi-Implicit Method for Pressure Linked Equations-Consistent
SIMPLER : Semi-Implicit Method for Pressure Linked Equations-Revised

LIST OF TABLES

Page Number

LIST OF FIGURES

Page Number

LIST OF SYMBOLS

J	: Jacobian of the transformation
k	: Turbulence kinetic energy
p	: Pressure
u, v	: Cartesian velocity components
$\mathbf{U_f, V_f}$	: Contravariant velocity fluxes in ξ and η directions
ε	: Turbulence dissipation rate
ξ, η	: General curvilinear coordinates
δξ, δη	: Distances between the grid nodes in the computational space
Δξ, Δη	: Distances between the cell faces in the computational space
ρ	: Density
μ	: Molecular viscosity
μ_t	: Turbulent viscosity
ω	: Turbulence specific dissipation rate

KOMPLEX GEOMETRİLERDE TÜRBÜLANSLI AKIŞIN SAYISAL ÇÖZÜMÜ

ÖZET

Bu çalışmada komplex geometrilerde türbülanslı akışın sayısal çözümü incelenmiştir. Sözkonusu akış iki boyutlu, sıkıştırılamaz, ve daimi bir türbülanslı akıştır. Hesaplamalar Sonlu hacimler Yöntemi kullanılarak genelleştirilmiş eğrisel koordinatlarda yapılmıştır. Yapısal bir ağ kullanılmış ve hücre merkezli bir ağ düzeni kullanılmıştır. Basıncın ve hızların hesaplanması için SIMPLE ve SIMPLEC yöntemi kullanılmıştır. Yapısal ağlarda hücre-merkezli ağ düzeni kullanılması ile ortaya çıkan fiziksel olmayan dalgalanmayı engellemek içim Momentum İnterpolasyon yöntemi uygulanmıştır.

Yazılan bilgisayar kodunda kullanılan türbülans modelleri duvar fonksiyonlarının kullanımını içeren standard k-ε modeli , Lam-Bremhorst'un düşük Reynolds sayılı k-ε modeli ve 1988 ve 1998 yıllarında Wilcox tarafından geliştirilen k-ω modelleridir. Fakat, düşük Reynolds sayılı k-ε modeli için, bu çalışma kapsamında bir yakınsamaya ulaşılamamıştır.

Sonunda, deneysel sonuçları bulunan iki farklı test prolemi seçilmiş ve sayısal olarak çözülmüştür. Elde edilen sayısal sonuçlar, deneysel sonuçlarla karşılaştırılmış ve her türbülans modelinin performansı incelenmiştir. 1998 k-ω modelinin, viskoz etkilerin çok önemli olduğu düşük Reynolds sayılı akışlarda en iyi sonucu verdiği tesbit edilmiştir. Öte yandan, yüksek Reynolds sayılı akışlarda da diğer iki model daha iyi sonuçlar vermektedir.

NUMERICAL COMPUTATION OF TURBULENT FLOW IN COMPLEX GEOMETRIES

SUMMARY

In this study, the numerical computation of turbulent flow in complex geometries has been accomplished. The considered flow is a 2-D, incompressible, and turbulent flow at steady state. Computation is done using finite volume method in generalized curvilinear coordinates. A structured grid and with a non-staggered (collocated) grid arrangement is used. SIMPLE and SIMPLEC algorithms have been used for the computation of pressure and velocities. Momentum interpolation method has been implemented to avoid the non-physical oscillation or so called red-black checkerboard splitting of the pressure field due to collocated grid arrangement.

The turbulence models employed in computer code are the standard k-ε model with wall functions, low Reynolds k-ε model of Lam-Bremhorst and two k-ω models developed by Wilcox in 1988 and 1998. However, with the low Reynolds model, convergence has not been achieved during this study.

In the end, two different test cases of which experimental data is available, has been chosen and solved numerically. The numerical results have been compared with the experimental ones and the performance of each turbulence model has been examined. It is concluded that for low Reynolds number flows, where the viscous effects play a very important role, 1998 k-ω model gives the best results. Though, the other two models give better predictions for high Reynolds number flows.

1 INTRODUCTION

Since, 1960s, there has been an increasing interest towards Computational Fluid Dynamics (CFD), with the development of computer technology. Especially after the invention of super computers in 1970s, and as the computing capacities get stronger in time, CFD has become more and more widespread among scientists. As, it was very expensive to set up and carry out experiments, scientists have tried to predict internal and external flows in numerical ways which are far less expensive, yet quite efficient at least in engineering aspects.

Today, CFD is a widely known and used technique and there are a lot of commercial CFD codes available to be used in many areas such as aerospace industry, food industry, glass industry etc. However, studies about CFD are still being carried on in every part of the world with full concentration. Scientists are trying to create a perfect code that can be applied to every physical problem in nature.

1.1 Literature Survey

Today, the "classical" or standard approach used most often in commercial software and research codes is Finite Volume Method (FVM). FVM, in fact, was originally developed as a special finite difference formulation. It is a method for representing and evaluating partial differential equations as algebraic equations. Similar to the finite difference method, values are calculated at discrete places on a meshed geometry. The numerical algorithm consists of the following steps **(Versteeg and Malalasekera, 1995)**:

- Formal integration of the governing equations of fluid flow over all the (finite) control volumes of the solution domain.
- Discretisation involves the substitution of a variety of finite-difference-type approximations for the terms in the integrated equation representing flow

process such as convection, diffusion sources. This converts the integral equations into a system of algebraic equations.

- Solution of the algebraic equations by an iterative method.

The first step, the control volume integration, distinguishes the FVM from all other CDF techniques. The resulting statements express the (exact) conservation of relevant properties for each finite size cell. This clear relationship between the numerical algorithm and the underlying physical conservation principle forms one of the main attractions of the FVM and makes its concepts much more simple to understand by engineers than finite element and spectral methods. The conservation of a general flow variable φ, for example a velocity component or enthalpy, within a finite control volume can be expressed as a balance between the various processes tending to increase or decrease it. In words we have:

Rate of change of φ in the C.V with respect to time	=	Net flux of φ due to convection into the C.V	+	Net flux of φ due to diffusion into the C.V	+	Net rate of creation of φ inside the C.V

In the set of fluid flow equations, pressure is the only variable that does not have a governing equation and especially in incompressible flows, it creates a big problem in the solution that there is not a direct link between pressure and velocity. With the general idea of solving the governing equations implicitly, various pressure schemes have been published to overcome this problem. One major distinction between the schemes is whether an equation for the pressure itself, an equation for a pressure correction, or both of these are solved. One method to handle this problem is the so-called "Semi-Implicit Method for Pressure Linked Equations" (SIMPLE) algorithm originally put forward by **Patankar and Spalding (1972)**. The essential feature is the replacement of the continuity equation (which does not contain the pressure) with a pressure correction equation, and subsequent sequential manipulations of the velocity field. Here, instead of solving an equation for the pressure itself, an equation for a pressure correction is solved. And once the pressure correction has been solved for, the velocities and pressures are upgraded accordingly. Still similar method of this kind was proposed by **Patankar (1980)** and is called SIMPLER (SIMPLE Revised). In this algorithm, the discretisized continuity equation is used to derive a discretisized equation for pressure, instead of a pressure correction equation as in

SIMPLE. Thus, the intermediate pressure field is obtained directly without the use of a correction. Velocities are, however, still obtained through the velocity corrections of SIMPLE. The SIMLEC (SIMPLE-Consistent) algorithm of **Van Doormall and Raithby (1984)** follows the same steps as the SIMPLE algorithm, with the difference that the momentum equations are manipulated so that the SIMPLEC velocity correction equations omit terms that are less significant than those omitted in SIMPLE. There are also other improved versions of SIMPLE, like PISO algorithm **(Isaa, 1986)**.

One other decision to be made is the grid arrangement to be used; staggered or non-staggered (collocated). When staggered grids are used, no interpolations are required for the velocity components at the faces of a pressure cell and it gives consistent pressure formulations **(Patankar, 1980)**. In this approach, the Cartesian velocity components are computed at the control volume faces through which the grid lines parallel to the corresponding Cartesian coordinate direction, pass. Although this approach is very successful in Cartesian grids, it loses its physical basis when applied to generalized coordinates, where the Cartesian velocity and the grid line directions are totally independent. The "equivalent" approach in a generalized coordinates formulation would be to locate the contravariant velocities at the control volume faces. The formulation for momentum equations using, contravariant velocities as dependent variables, however, incurs significant increases in complexity and may create non-conservative errors when the grid is not smooth **(Shyy and Vu, 1991)**.

An alternative is to use a collocated grid arrangement where all the variables are set at the same set of grid points and are stored in the same control volume. The collocated arrangement was out of favor for a long time for incompressible flow computation due to the difficulties with pressure-velocity coupling and the occurrence of oscillations in the pressure. The problem is that, storing both the pressure and velocities at the same grid point will cause non-physical oscillation or so-called red-black checkerboard splitting of the pressure field. This undesirable behavior stems from the fact that the resulting equations couple the pressure and velocities only at alternate nodes if a linear interpolation is used to express the gradients of pressure in the momentum equations and the variations of velocity in the continuity equation. To solve this problem, **Rhie and Chow (1983)** proposed a scheme based on momentum interpolation, and their approach resulted in a

revolution on the use of collocated grids. In this scheme, momentum equations are solved at the main grid points for Cartesian velocity components and the cell-face velocities are obtained by the interpolation of the momentum equations on the neighboring nodes. This original method is then further refined and extended to be used in general curvilinear coordinates by **Miller and Schmidt (1988)**.

Almost all fluid flow which we encounter in daily life is turbulent. Typical examples are flow around (as well as in) cars, aeroplanes and buildings. Thus, it excited the scientists interest to understand the physics of turbulence and then to model it somehow. If we accept the time-averaged Navier-Stokes equation as the origin of turbulence modeling, this takes us to back to the end of the nineteenth century when **Reynolds (1895)** published results of his research on turbulence. The earliest attempts at developing a mathematical description of turbulent stress sought to mimic the molecular gradient-diffusion process. In this spirit **Boussinesq (1877)** introduced the concept of a so-called eddy viscosity. However, neither Reynolds nor Boussinesq attempted a solution of the Reynolds-averaged Navier-Stokes equation in any systematic manner. Much of the physics of viscous flows was a mystery in the nineteenth century, and further progress awaited Prandtl's discovery of the boundary layer in 1904. focusing upon turbulent flows, **Prandtl (1925)** introduced the mixing length (an analogy of the mean free path of the gas) and a straightforward prescription for computing the eddy-viscosity in terms of the mixing length. Important contributions were also made by several authors, most notably by **von Karman (1930)**. In modern terminology, we refer to a model based on the mixing-length hypothesis as an algebraic model or a zero-equation model of turbulence. By definition an n-equation model signifies a model that requires solution of n additional differential transport equations in addition to those expressing conservation of mass, momentum, and energy for the mean flow.

To improve the ability to predict properties of turbulent flows and to develop a more realistic mathematical description of the turbulent stresses, **Prandtl (1945)** postulated a model in which the eddy viscosity depends upon the kinetic energy of turbulent fluctuations, k. he proposed a modeled partial-differential equation approximating the exact equation for k. thus was born the concept of the so-called one-equation model of turbulence.

Kolmogorov (1942) introduced the first complete model of turbulence. In addition to having a model equation for k, he introduced a second parameter ω that he referred to as "the rate of dissipation of energy in unit volume and time." The reciprocal of ω serves as a turbulence time scale, while $k^{1/2}\omega$ serves as the analog of the mixing length and $k\omega$ is the analog of the dissipation rate, ε. In this model, known as a *k*-ω model, ω satisfies a differential equation somewhat similar to the equation for k. the model is thus termed a two-equation model of turbulence.

While Kolmogorov's *k*-ω model was the first of this type, it remained in obscurity until the coming of the computer. By far, the most extensive work on two-equation models has been done by **Launder and Spalding (1972)** and a continuing success of students and colleagues. Launder's *k*-ε model is as well-known as the mixing-length model is the most widely used two-equation model. With no prior knowledge of Kolmogorov's work, **Saffman (1970)** formulated a *k*-ω model that enjoys advantages over the *k*-ε model, especially for integrating through the viscous sublayer and for predicting effects of adverse pressure gradient. **Wilcox and Alber (1972)**, **Saffman and Wilcox (1974)**, **Wilcox and Traci (1976)**, **Wilcox and Rubesin (1980)**, and **Wilcox (1988)**, for example, have pursued further development and application of *k*-ω models. And later **Wilcox (1998)** introduced a new version of the *k*-ω model with a significant improvement over that described in the first edition.

On the other hand, **Chou (1945)** and **Rotta (1951)** laid the foundation for turbulence models that obviate the use of the Boussinesq approximation. Rotta devised a plausible model for the differential equation governing evaluation of the tensor that represents the turbulent stresses, i.e., the Reynolds-stress tensor. Such models are most appropriately described as stress-transport models. By 1970s, sufficient computer resources became available to permit serious development of this class of model. The most notably efforts were those of **Donaldson (1968)**, **Daly and Harlow (1970)** and **Launder, Reece and Rodi (1975)**. The latter has become the baseline stress-transport model: more recent contributions by **Lumley (1978)**, **Speziale (1985, 1987, 1991)** and **Reynolds (1987)** have added mathematical rigor to the closure process. However, because of the large number of equations and complexity involved, they have found their way into a relatively small number of applications compared to algebraic and two-equation models.

2 GOVERNING EQUATIONS

In this chapter, the governing equations of a 2-D, turbulent, incompressible flow at steady-state will be presented. Since the main property of the computer code written as a part of this masters study is the usage of generalized curvilinear coordinates, equations will be first presented in Cartesian coordinates and then in generalized curvilinear coordinates.

2.1 General Convection-Diffusion Equation Form

The momentum, and turbulence equations are all considered to be specific cases of a general convection-diffusion scalar transport equation. Therefore, it is appropriate to give the general convection-diffusion equation before proceeding into the specific forms (in conservative form):

$$\frac{\partial \rho\phi}{\partial t}+\frac{\partial \rho u\phi}{\partial x}+\frac{\partial \rho v\phi}{\partial y}+\frac{\partial \rho w\phi}{\partial z}=\frac{\partial}{\partial x}\left(\Gamma_x\frac{\partial \phi}{\partial x}\right)+\frac{\partial}{\partial y}\left(\Gamma_y\frac{\partial \phi}{\partial y}\right)+\frac{\partial}{\partial z}\left(\Gamma_z\frac{\partial \phi}{\partial z}\right)+S_\phi \qquad \textbf{(2.1)}$$

unsteady convection diffusion source

In order to obtain a numerical solution on a curvilinear grid, equations in Cartesian coordinates should be transformed into general curvilinear coordinates. For the details of this transformation, reader is referred to the thesis of **Anton H. Basson (1992)**. Below can be seen the final form of the transport equation after the transformation:

$$\begin{aligned}&\frac{\partial}{\partial \xi}\left(\rho JG_1\phi\right)+\frac{\partial}{\partial \eta}\left(\rho JG_2\phi\right)=\\&\frac{\partial}{\partial \xi}\left[\Gamma J^{-1}\left(\alpha\frac{\partial \phi}{\partial \xi}+\theta_1\frac{\partial \phi}{\partial \eta}\right)\right]+\frac{\partial}{\partial \eta}\left[\Gamma J^{-1}\left(\theta_1\frac{\partial \phi}{\partial \xi}+\beta\frac{\partial \phi}{\partial \eta}\right)\right]+S_\phi J\end{aligned} \qquad \textbf{(2.2)}$$

where JG_1 and JG_2 are contravariant velocity fluxes , and G_1 and G_2 are contravariant velocity components along ξ and η directions respectively. Contravariant velocity fluxes will be used as dependent variables in the momentum equations.

$$\rho JG_1 = \rho\left(uy_\eta - vx_\eta\right) = U_f \qquad \text{contravariant velocity flux in } \xi \text{ direction} \qquad \textbf{(2.2a)}$$

$$\rho JG_{21} = \left(-uy_\xi + vx_\xi\right) = V_f \qquad \text{contravariant velocity flux in } \eta \text{ direction} \qquad \textbf{(2.2b)}$$

$$\alpha = y_\eta^{\,2} + x_\eta^{\,2}$$

$$\beta = y_\xi^{\,2} + x_\xi^{\,2} \qquad \textbf{(2.2c)}$$

$$\theta_1 = -y_\eta y_\xi - x_\eta x_\xi$$

$$J = x_\xi y_\eta - x_\eta y_\xi$$

In the following subsections, the momentum and the turbulence equations will be presented by substituting the dependent variable with proper variables.

2.1.1 Momentum equations

The momentum equation is a statement of Newton's Second Law and relates the sum of the forces acting on an element of fluid to its acceleration or rate of change of momentum. The details of the general development of the equation are given in many fluid mechanics texts **(White, 1974)**

In this section, with the approximation of a 2-D, incompressible steady-state flow, and with constant flow properties, the general form of the momentum equations will be presented. However, as a general tendency in CFD, pressure term is taken out of the source term and written explicitly:

$$\frac{\partial \rho uu}{\partial x} + \frac{\partial \rho vu}{\partial y} + = \frac{\partial}{\partial x}\left(\mu \frac{\partial u}{\partial x}\right) + \frac{\partial}{\partial y}\left(\mu \frac{\partial u}{\partial y}\right) + \frac{\partial p}{\partial x} + S_u \qquad \textbf{(2.3)}$$

Likewise, v momentum equation is:

$$\frac{\partial \rho uv}{\partial x} + \frac{\partial \rho vv}{\partial y} + = \frac{\partial}{\partial x}\left(\mu \frac{\partial v}{\partial x}\right) + \frac{\partial}{\partial y}\left(\mu \frac{\partial v}{\partial y}\right) + \frac{\partial p}{\partial y} + S_v \qquad \textbf{(2.4)}$$

2.2 Turbulence Equations

Mainly two different turbulence models have been implemented in the computer code, namely the k-ε and k-ω models. For k-ε model, wall-function approach **(Launder & Spalding, 1972)** and low-Reynolds approach of **Lam-Bremhorst (1981)**, and for k-ω model, two versions of Wilcox's k-ω have been chosen. Before going into the details of these two models, the base of those models, Reynolds-Averaged Equations will be analyzed.

2.2.1 Reynolds-averaged equations

The beginning step of turbulence modeling is the time-averaged Navier-Stokes equations and the origin of this approach dates back to the end of nineteenth century with Reynolds's studies on turbulence in 1895. Naturally, the starting point of the derivation is the conservation equations of mass and momentum. For a 2-D, incompressible, constant-property flow, they are as follows:

$$\frac{\partial u_i}{\partial x_i} = 0 \qquad \textbf{(2.5)}$$

$$\rho \frac{\partial u_i}{\partial t} + \rho \frac{\partial}{\partial x_j}\left(u_j u_i\right) = -\frac{\partial p}{\partial x_i} + \frac{\partial t_{ji}}{\partial x_j} \qquad \textbf{(2.6)}$$

where μ is the molecular viscosity and t_{ij} is the viscous stress tensor, defined by

$$t_{ij} = 2\mu . s_{ij} \qquad \textbf{(2.7)}$$

and s_{ij} is the strain-rate tensor:

$$s_{ij} = \frac{1}{2}\left(\frac{\partial u_i}{\partial x_j} + \frac{\partial u_j}{\partial x_i}\right) \qquad \textbf{(2.8)}$$

At this point, defining the instantaneous velocity, $u_i(x,t)$ in terms of a mean, $U_i(x,t)$ and a fluctuating part, $u'_i(x,t)$:

$$u_i(x,t) = U_i(x) + u_i'(x,t) \qquad \textbf{(2.9)}$$

instantaneous — mean; fluctuating

and time (ensemble) averaging equations (2.5) and (2.6), "Reynolds Averaged equations of motion in conservation form" are obtained:

$$\frac{\partial U_i}{\partial x_i} = 0 \qquad \textbf{(2.10)}$$

$$\rho \frac{\partial U_i}{\partial t} + \rho \frac{\partial}{\partial x_j}\left(U_j U_i\right) = -\frac{\partial p}{\partial x_i} + \frac{\partial}{\partial x_j}\left(2\mu . S_{ij} - \rho . \overline{u_j' u_i'}\right) \qquad \textbf{(2.11)}$$

Reynolds-Averaged Navier-Stokes (RANS) Equations

Reynolds-Stresses-tensor

Time-averaged and instantaneous mass-conservation equations are the same in shape, only difference being the replacement of the instantaneous velocities by the mean ones as a result of the averaging. However for the momentum equations, aside from the replacement of the instantaneous velocities, there is an extra term in the time-averaged equation due to the fluctuations in turbulence, $\rho . \overline{u_j' u_i'}$, namely the Reynolds-stress tensor.

"Herein lies the fundamental problem of turbulence. In order to compute all mean-flow properties of the turbulent flow under consideration, a prescription is needed for computing $\rho . \overline{u_j' u_i'}$." **(Wilcox,1998)**

So, at this point, for a 3-D flow, there are 10 unknowns; 4 from mean flow (P,U,V,W), and 6 from turbulence ($\overline{uu}, \overline{uv}, \overline{uw}, \overline{vv}, \overline{vw}, \overline{ww}$). On the other hand, there are only 4 equations available (3 momentum + continuity); meaning that 6 more

equations are needed to close the system. This is the famous turbulence closure problem.

Over the years, there have been different approaches to this problem as mentioned in the literature survey of this thesis. Shortly, mentioning here again, the first attempt was to model the Reynolds stress as a function of the mean-flow equations (zero-equation models). Later other scientists developed one-equation models, where they created an extra transport equation, and two-equation models, where two-extra equations are developed in order to close the system. Apart from these, in Stress-Transport models, 6 more transport equation is developed for each Reynolds-stress component by taking the moment of the Navier-Stokes equations.

The main concentration of this thesis is the two-equation models with Boussinesq Eddy-viscosity assumption.

2.2.2 Boussinesq assumption

In eddy viscosity turbulence models, Reynolds-stresses are expressed in terms of mean-flow equations with a proportionality coefficient in between named as the turbulent viscosity. This approach is called as the Boussinesq assumption , and in analogy with Stokes' postulate for laminar flows, it assumes that the principal axes of the Reynolds stress-tensor are coincident with those of mean strain-rate tensor at all points in a turbulent flow **(Boussinesq,1877)**.

$$\rho.\overline{u_i' u_j'} = -\mu_t \left(\frac{\partial U_i}{\partial x_j} + \frac{\partial U_j}{\partial x_i} \right) + \frac{2}{3}\delta_{ij}\rho k \qquad \textbf{(2.12)}$$

where, μ_t is the turbulent or eddy viscosity to be defined accordingly in different turbulence models.

2.3 *k*-ε model

By far, the most popular two-equation model is the *k*-ε model. Several scientists helped progress of the model such as **Chou (1945)**, **Davidov (1961)**, and **Harlow and Nakayama (1968)**. However, the most famous paper accepted today as the source of the standard the *k*-ε model was published by **Jones and Launder (1972)**.

And **Launder and Sharma (1974)** indicated the model's closure coefficients that are still being used by most of the researches today. The standard *k-ε* model is as follows:

Turbulence kinetic energy, k equation:

$$\frac{\partial}{\partial x}(\rho U k)+\frac{\partial}{\partial y}(\rho V k)=\frac{\partial}{\partial x}\left[\left(\mu+\frac{\mu_t}{\sigma_k}\right)\frac{\partial k}{\partial x}\right]+\frac{\partial}{\partial y}\left[\left(\mu+\frac{\mu_t}{\sigma_k}\right)\frac{\partial k}{\partial y}\right]+P_k-\rho\varepsilon \qquad \textbf{(2.13)}$$

Dissipation rate, ε equation:

$$\frac{\partial}{\partial x}(\rho U \varepsilon)+\frac{\partial}{\partial y}(\rho V \varepsilon)=\frac{\partial}{\partial x}\left[\left(\mu+\frac{\mu_t}{\sigma_k}\right)\frac{\partial \varepsilon}{\partial x}\right]+\frac{\partial}{\partial y}\left[\left(\mu+\frac{\mu_t}{\sigma_k}\right)\frac{\partial \varepsilon}{\partial y}\right]+\frac{\varepsilon}{k}\left(C_{\varepsilon 1}P_k-C_{\varepsilon 2}\rho\varepsilon\right) \qquad \textbf{(2.14)}$$

with the closure coefficients being:

$$C_{\varepsilon 1}=1.44 \qquad C_{\varepsilon 2}=0.92 \qquad C_{\mu}=0.09 \qquad \sigma_k=1.0 \qquad \sigma_{\varepsilon}=1.3 \qquad \textbf{(2.15)}$$

and turbulence viscosity, μ_t defined as:

$$\mu_t=C_{\mu}\frac{k^2}{\varepsilon} \qquad \textbf{(2.16)}$$

In these equations, the term P_k is the source term. It is defined as follows:

$$P_k=-\rho\overline{u_i'u_j'}\frac{\partial U}{\partial x_j} \qquad \textbf{(2.17)}$$

and it is calculated with the insertion of Boussinesq assumption (eq.(2.12)) into the Reynolds-stress term. Doing so, source term gets the following final shape for flows away from the wall:

$$P_k = \mu_t \left(\frac{\partial U_i}{\partial x_j} + \frac{\partial U_j}{\partial x_i} \right) \frac{\partial U_i}{\partial x_j} - \frac{2}{3} \delta_{ii} \rho k \qquad \textbf{(2.18)}$$

2.3.1 Wall-functions

The standard *k-ε* model has been developed for regions with sufficiently high Reynolds-numbers. Because of this, it is not valid in regions very close to the wall where viscous effects are important and the local Reynolds-numbers are relatively low. For wall-bounded flows, one approach for this problem is to use the standard equations of *k-ε* far from the wall, in fully-developed turbulent regions and to use the empirical wall-functions to bridge the distance to the wall and in this section, information about this approach will be given. Another approach named as low-Reynolds turbulence modeling will be presented in the following sections.

2.3.1.1 The use of wall functions

On figure (2.1), a near wall situation can be seen. As explained above, for the fully-developed turbulent part of the flow, that is, for the regions away from the solid boundaries, standard k-ε equations are used. Wall functions are used to link this turbulent zone and the wall and they are applied to the first grid point above the wall, P.

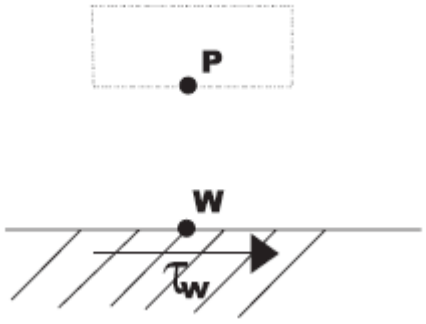

Figure 2.1: Near Wall Situation

In wall-functions approach, the vicinity of the wall is assumed to be made up of a two-layer structure; a viscous sublayer very near the wall, and a log-layer just above it. With this assumption, for a fully developed turbulent flow near a no-slip wall, the normalized tangential velocity can be written as follows **(White, 1974)**:

$$U^+ = \frac{U^t}{u_\tau} = \frac{1}{\kappa}\ln\left(Ey^+\right) \qquad y^+ > 11.63 \qquad \textbf{(2.19)}$$

$$U^+ = y^+ \qquad y^+ < 11.63 \qquad \textbf{(2.20)}$$

where

$$y^+ = \frac{u_\tau y}{\nu} \qquad u_\tau = \sqrt{\frac{\tau_{wall}}{\rho}} \qquad \textbf{(2.21)}$$

In these equations, κ, the von Karman constant has the value 0.4187 and the constant E is assigned to be 9.793 for smooth walls. With this first definition of wall functions, researches encountered some problems in near flow separation regions. The reason is that in these regions, the friction velocity, u_τ goes to zero causing y^+ also to be so. To overcome this problem, new assumptions have been made as below:

- Couette flow
- Local equilibrium between production and dissipation
- Constant stress layer near the wall

Using these assumptions, the wall shear stress is related to the turbulent kinetic energy and defined as:

$$\frac{\tau_{wall}}{\rho} = \sqrt{C_\mu}k \qquad \textbf{(2.22)}$$

or equivalently

$$u_\tau = C_\mu^{\frac{1}{4}}\sqrt{k} \qquad \textbf{(2.23)}$$

This new form avoids the singularity problem, since k does not become zero at separation, and neither does τ_{wall}. Below can be seen a different presentation of τ_{wall} with the new definitions:

$$\tau_{wall} = \tau_{vis}\left(\frac{y^+}{U^+}\right) \quad \textbf{(2.24)}$$

where

$$\tau_{vis} = \mu\frac{u^t}{y_p} \quad \textbf{(2.25)}$$

$$y^+ = \frac{\rho C_\mu^{\frac{1}{4}} k^{\frac{1}{2}} y_p}{\mu} \quad \textbf{(2.26)}$$

Inserting the definitions above shear stress (in the log layer), equation (2.24) can also be expressed as:

$$\tau_{wall} = \frac{\rho\kappa C_\mu^{\frac{1}{4}} k^{\frac{1}{2}}}{\ln\left(Ey^+\right)} u^t \quad \textbf{(2.27)}$$

2.3.1.2 k and ε at a near wall node

There are several techniques to solve the turbulent kinetic energy and dissipation rate equation at a near wall node. As a general tendency, the dissipation rate, ε at near-wall nodes is most often assigned a value, making the same local equilibrium assumption, instead of solving the equation governing it. On the other hand, for the turbulent kinetic energy, k, there is not a single common approach. It is either assigned a value **(Patel et al., 1985, Sondak and Pletcher, 1995)** or computed using its governing equation **(Launder and Spalding, 1974)**. In this thesis, this second approach has been implemented, and source terms in the k-equation (production and dissipation of k) have been predicted using the assumptions made in the definition of wall functions.

Performing integration from the wall to the node P and assuming constant τ_{wall} in the near wall region, the production of k term, P_k is defined as follows in the near wall region:

$$P_k = \tau_{wall} \frac{u_p^{\ t}}{y_p} \tag{2.28}$$

and by introducing the definitions, it gets the following form:

$$P_k = \frac{\rho C_\mu^{\frac{1}{4}} \sqrt{k} U_p^{\ t} \kappa}{\ln\left(E y^+\right)} \Delta U \tag{2.29}$$

Consistent with the approximation of the production term given above, the dissipation termin k equation, $-\rho\varepsilon$ is estimated as follows:

$$-\rho\varepsilon = -\frac{C_\mu^{\frac{3}{4}} k_p^{\frac{3}{2}}}{\kappa y_p} \ln\left(E y_p^{\ +}\right) \tag{2.30}$$

As explained above in the introduction part of this section, ε-equation is not solved at a near wall node. Instead of this, ε is fixed according to:

$$\varepsilon = \frac{u_\tau^{\ 3}}{\kappa y} = \frac{C_\mu^{\frac{3}{4}} k_p^{\frac{3}{2}}}{\kappa y_p} \tag{2.31}$$

which is a direct consequence of using the definition of friction velocity with the log-law (eq. (2.19)), with the assumption of local equilibrium between the production and dissipation of turbulent kinetic energy.

2.3.2 Low-Reynolds number models

Another technique to capture the flow in the near wall region is to use a so-called low-Reynolds number model. In this model, instead of using wall-functions in the near wall region and standard equations in the outer fully-developed turbulent region, same equations are used throughout the whole domain (integration through the viscous sublayer). By the help of the viscous damping functions introduced to the turbulent kinetic energy and dissipation rate equations, viscous effects dominating the near wall region are taken into consideration.

Throughout the history, several different *k-ε* low Reynolds number models have been developed by scientists, some of which are by **Jones and Launder (1972)**, **Launder and Sharma (1974)**, **Lam and Bremhorst (1981)**. In this thesis, Lam and Bremhorst's model developed in 1981 has been implemented in the code. Below are the equations and closure coefficients and the damping functions of the model:

$$\frac{\partial}{\partial x}(\rho U k)+\frac{\partial}{\partial y}(\rho V k)=\frac{\partial}{\partial x}\left[\left(\mu+\frac{\mu_t}{\sigma_k}\right)\frac{\partial k}{\partial x}\right]+\frac{\partial}{\partial y}\left[\left(\mu+\frac{\mu_t}{\sigma_k}\right)\frac{\partial k}{\partial y}\right]+P_k-\rho\varepsilon \qquad \textbf{(2.32)}$$

$$\frac{\partial}{\partial x}(\rho U\tilde{\varepsilon})+\frac{\partial}{\partial y}(\rho V\tilde{\varepsilon})=\frac{\partial}{\partial x}\left[\left(\mu+\frac{\mu_t}{\sigma_k}\right)\frac{\partial \tilde{\varepsilon}}{\partial x}\right]+\frac{\partial}{\partial y}\left[\left(\mu+\frac{\mu_t}{\sigma_k}\right)\frac{\partial \tilde{\varepsilon}}{\partial y}\right]+\frac{\tilde{\varepsilon}}{k}\left(C_{\varepsilon 1}f_1P_k-C_{\varepsilon 2}f_2\rho\tilde{\varepsilon}\right) \qquad \textbf{(2.33)}$$

In the dissipation rate equation, the newly introduced variable, $\tilde{\varepsilon}$ is related to the dissipation, ε by:

$$\varepsilon=\varepsilon_0+\tilde{\varepsilon} \qquad \textbf{(2.34)}$$

In the equations, (2.32) and (2.33), there are five empirical damping functions, f_1, f_2, f_μ, ε_0 and E. These functions depend upon one or more of the following three dimensionless parameters:

$$\mathrm{Re}_\tau=\frac{k^2}{\tilde{\varepsilon}\nu} \qquad R_y=\frac{k^{1/2}y}{\nu} \qquad y^+=\frac{u_\tau y}{\nu} \qquad \textbf{(2.35)}$$

and the damping functions and closure coefficients of Lam-Bremhorst model are as follows:

<u>Lam-Bremhorst Model</u>

$$f_\mu=\left(1-e^{-0.0165R_y}\right)^2\left(1+20.5/\mathrm{Re}_\tau\right) \qquad \textbf{(2.36a)}$$

$$f_1=1+\left(0.05/f_\mu{}^3\right) \qquad \textbf{(2.36b)}$$

$$f_2 = 1 - e^{-\mathrm{Re}_T^{\,2}} \qquad \textbf{(2.36c)}$$

$$\varepsilon_0 = 0 \qquad \textbf{(2.36d)}$$

$$C_{\varepsilon 1} = 1.44 \qquad C_{\varepsilon 2} = 0.92 \qquad C_\mu = 0.09 \qquad \sigma_k = 1.0 \qquad \sigma_\varepsilon = 1.3 \qquad \textbf{(2.36e)}$$

2.4 *k-ω* model

In 1942 **Kolmogorov (1942)** proposed the first two-equation turbulence model. His two turbulence parameters were the turbulent kinetic energy, k, as in k-ε models and the dissipation per unit turbulence kinetic energy, ω. After this first version of k- ω, several contributions were made to the model by several scientists as mentioned in the literature survey part. The contributions and improvements were especially for the ω equation and ω equation has changed as the model has evolved throughout the history. In this thesis, two versions of Wilcox's k- ω model that he developed in 1988 **(Wilcox, 1988)** and in 1998 **(Wilcox, 1998)** will be discussed.

The governing equations of these two models are completely the same. The differences are in the coefficients as shown below:

Turbulence kinetic energy, k equation:

$$\frac{\partial}{\partial x}(\rho U k) + \frac{\partial}{\partial y}(\rho V k) = \frac{\partial}{\partial x}\left[\left(\mu + \frac{\mu_t}{\sigma^{\omega}{}_k}\right)\frac{\partial k}{\partial x}\right] + \frac{\partial}{\partial y}\left[\left(\mu + \frac{\mu_t}{\sigma^{\omega}{}_k}\right)\frac{\partial k}{\partial y}\right] + P_k - \rho\beta^* k\omega \qquad \textbf{(2.37)}$$

Specific Dissipation Rate, ω equation:

$$\frac{\partial}{\partial x}(\rho U \omega) + \frac{\partial}{\partial y}(\rho V \omega) = \frac{\partial}{\partial x}\left[\left(\mu + \frac{\mu_t}{\sigma_\omega}\right)\frac{\partial \omega}{\partial x}\right] + \frac{\partial}{\partial y}\left[\left(\mu + \frac{\mu_t}{\sigma_\omega}\right)\frac{\partial \omega}{\partial y}\right] + \alpha\frac{\omega}{k}P_k - \rho\beta\omega^2 \qquad \textbf{(2.38)}$$

Kinematic Eddy Viscosity:

$$\upsilon_t = \mu_t / \rho = k/\omega \qquad \textbf{(2.39)}$$

Closure Coefficients:

Wilcox-1988:

$$\alpha = 0.56 \quad \beta = 0.075 \quad \beta^* = 0.09 \quad \sigma^{\omega}{}_k = 2 \quad \sigma_\omega = 2 \qquad \textbf{(2.40)}$$

Wilcox-1998:

$$\alpha = 0.52 \quad \beta = \beta_0 f_\beta \quad \beta^* = \beta_o^* f_{\beta^*} \quad \sigma^{\omega}{}_k = 2 \quad \sigma_\omega = 2 \qquad \textbf{(2.41a)}$$

$$\beta_o = 0.072 \qquad f_\beta = \frac{1+70\chi_\omega}{1+80\chi_\omega} \qquad \chi_\omega = 0 \ \text{(for 2-D flows)} \qquad \textbf{(2.41b)}$$

$$\beta_o^* = 0.09 \qquad f_{\beta^*} = \begin{cases} 1 & \chi_k \le 0 \\ \dfrac{1+680\chi_k{}^2}{1+400\chi_k{}^2}, & \chi_k > 0 \end{cases} \qquad \chi_k \equiv \frac{1}{\omega^3}\frac{\partial k}{\partial x_j}\frac{\partial \omega}{\partial x_j} \qquad \textbf{(2.41c)}$$

The most important difference in the new version k-ω is in the coefficients of the dissipation terms, $\beta*$ and β. The functions $f_{\beta*}$ and f_β, which depend upon χ_k and χ_ω do not appear in Wilcox-1988 model. Also the values of α and β_0 are a bit different from the values used at Wilcox 1988 model.

The most important property of the first model, Wilcox-1988 is that it predicts boundary layer properties that are in very good agreement with measurements. With changes, Wilcox-1998 model still does so, because χ_k and χ_ω are very small close to a solid boundary. Therefore, they have a very little effect in those regions. However, with these changes, this new version dramatically improves predictive accuracy of Wilcox-1988 model for free shear flows. And this makes the new model applicable to both wall-bounded and free shear flows.

2.4.1 Integration through the viscous sublayer

The most distinctive property of *k-ω* model is the integration through the viscous sublayer without the need for viscous damping functions. Actually, wall-functions can also be used in the near wall region, like *k-ε* model, but integration through the viscous sublayer gives better results. Here are the equations for this near wall-

integration, details of which can be found in "Turbulence Modeling for CFD" by David C. Wilcox **(Wilcox, 1998)**:

On the wall surface, ω is calculated by the following expression:

$$\omega = \frac{u_\tau^{\,2}}{\nu_w} S_R \qquad \text{at} \qquad y=0 \tag{2.42}$$

where

$$S_R = \left(50/k_s^{+}\right)^2 \quad , k_s^{+} < 25 \tag{2.43}$$

The quantity $k_s^{+} = u_\tau k_s / \nu_w$ is the scaled surface-roughness height, k_s being the roughness height.

In order to simulate a smooth surface, k_s^{+} is required to be less than 5, and for a perfectly-smooth wall, it can be assigned directly to be equal to1.

Finally, ω equation is not solved in the near-wall region. Instead, for y^+ values less than 2.5, it is calculated by the following equation:

$$\omega = \frac{\omega_w}{\left(1+\sqrt{\frac{\beta_o \omega_w}{6\nu_w}}\right)^2} \qquad , \quad y^+ < 2.5 \tag{2.44}$$

3 DISCRETIZATION

In this chapter, the discretization of the governing equations will be given using the finite-volume approach. As the general convection-diffusion equation presented in chapter 2 is analogous to most of the differential equations in fluid dynamics problems, its discretization will be performed.

3.1 Finite-Volume Method

The basics of the finite-volume method are to divide the computational domain into a set of control volumes and to express the conservation laws in an integral form for each of these control volumes. This control-volume approach has the advantage of preserving conservation properties, which is extremely desirable for engineering applications where overall balance of mass, momentum and other quantities are often of prime importance.

Naturally, the grid to be used for the discretization, in other words, the computational domain is very important. In context of this thesis, physical domain of the real problem is transformed into a rectangular computational domain every time as shown in figure 3.1. In the figure, the crosses are the boundaries of the control volumes and the dots placed in the center of those four crosses surrounding the control volume are the computation points (grid points) of the dependent variables. The x direction in the physical domain is replaced by ξ in the computational domain; and y by η.

In the computational domain, the distances between the grid points are denoted by $\delta\xi$ and $\delta\eta$ in ξ and η directions respectively. Meanwhile, $\Delta\xi$ and $\Delta\eta$ denote distance between the faces of the control volumes. As it will be seen further in this chapter, these four quantities, $\delta\xi$, $\delta\eta$, $\Delta\xi$, $\Delta\eta$ appear in the discretized transformed equations. Therefore, in order to simplify calculations, it would be appropriate to assign them all to be equal to unity no matter what their corresponding values in the physical domain are.

One other specific property of the grid for this study is the use of ghost cells at the boundaries. In figure 3.1, the solid lines symbolize the corresponding physical borders on the computational plane. And in a way, the crosses are the centers of the volumes created by the dashed lines of the computation points. The special case here is that the dashed lines and therefore the dots located at the very outer edge of the computational domain have no meaning on physical plane. They are completely imaginary. They are given the proper values, taking the physical boundaries into consideration, and they help simplify things in the boundaries as they cancel "half" control-volumes that would exist otherwise.

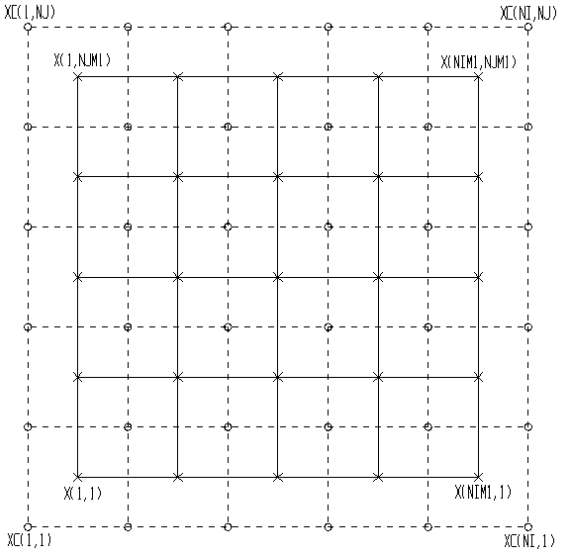

Figure 3.1: Computational Space

Last of all, the grid used in this thesis is arranged in a non-staggered way. That is, the dependent variables are all stored at the same grid points. The uppercase letters P, E, W, N and S indicate the grid points whereas the lowercase letters e, w, n and s, indicate the cell faces relative to point P (figure 3.2).

3.2 Discretization of the General Convection-Diffusion Equation

The general convection-diffusion equation in curvilinear coordinates (eq. (2.2)) presented in section 2.1 can be written with a little difference like this:

$$\frac{\partial}{\partial \xi}\left(U_f \phi\right)+\frac{\partial}{\partial \eta}\left(V_f \phi\right)= \\ \frac{\partial}{\partial \xi}\left[\Gamma J^{-1}\left(\alpha \frac{\partial \phi}{\partial \xi}+\theta_1 \frac{\partial \phi}{\partial \eta}\right)\right]+\frac{\partial}{\partial \eta}\left[\Gamma J^{-1}\left(\theta_1 \frac{\partial \phi}{\partial \xi}+\beta \frac{\partial \phi}{\partial \eta}\right)\right]+S_\phi J \qquad \textbf{(3.1)}$$

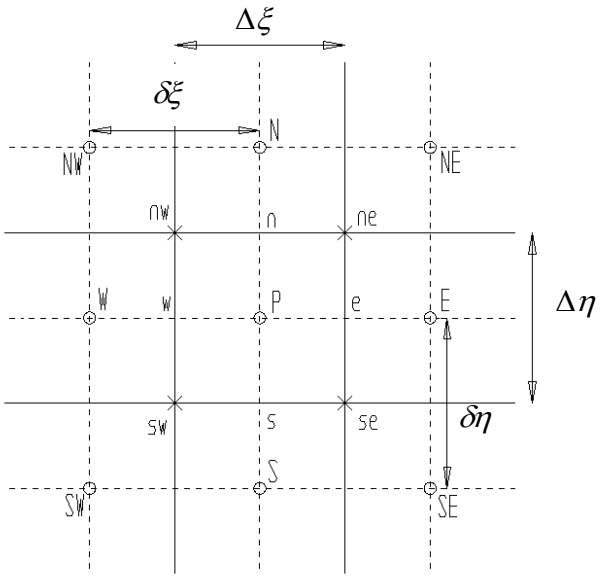

Figure 3.2: Grid Arrangement

The difference here is that contravariant velocity fluxes that are defined before in section 2.1 are used directly in the convection terms. Other coefficients are the same as before.

The discretization form of this general governing equation can be obtained by integrating equation (3.1) over the control volume on the $\xi-\eta$ plane.

$$\begin{aligned}&\iint_{\forall}\left[\frac{\partial}{\partial\xi}\left(U_f\phi\right)+\frac{\partial}{\partial\eta}\left(V_f\phi\right)\right]d\xi d\eta=\\&\iint_{\forall}\frac{\partial}{\partial\xi}\left[\Gamma J^{-1}\left(\alpha\frac{\partial\phi}{\partial\xi}+\theta_1\frac{\partial\phi}{\partial\eta}\right)\right]d\xi d\eta+\iint_{\forall}\frac{\partial}{\partial\eta}\left[\Gamma J^{-1}\left(\theta_1\frac{\partial\phi}{\partial\xi}+\beta\frac{\partial\phi}{\partial\eta}\right)\right]d\xi d\eta\\&+\iint_{\forall}S_\phi J d\xi d\eta\end{aligned}\qquad\textbf{(3.2)}$$

where $\forall$ denotes the control volume. Now, applying the Green theorem, equation (3.2) is given the following form:

$$\begin{aligned}&\oint_{cs}\left(U_f\phi d\eta-V_f\phi d\xi\right)=\oint_{cs}\left[\Gamma J^{-1}\left(\alpha\frac{\partial\phi}{\partial\xi}+\theta_1\frac{\partial\phi}{\partial\eta}\right)\right]d\eta+\oint_{cs}\left[\Gamma J^{-1}\left(\theta_1\frac{\partial\phi}{\partial\xi}+\beta\frac{\partial\phi}{\partial\eta}\right)\right]d\xi\\&+\iint_{\forall}S_\phi J d\xi d\eta\end{aligned}\qquad\textbf{(3.3)}$$

In the above equation, "cs" denotes the surface of the given volume $\forall$. Now, if this equation is discretized over the control-volume cell in the computational space shown in figure 3.1 and the line integrals are taken accordingly,

$$\begin{aligned}&\left(U_f\phi.\Delta\eta\right)_w^e+\left(V_f\phi.\Delta\xi\right)_s^n=\left[\Gamma J^{-1}\left(\alpha\phi_\xi+\theta_1\phi_\eta\right)\Delta\xi\right]_s^n+\left[\Gamma J^{-1}\left(\theta_1\phi_\xi+\beta\phi_\eta\right)\Delta\eta\right]_w^e\\&+S_\phi J\Delta\xi\Delta\eta\end{aligned} \tag{3.4}$$

Here, the quantities, ϕ_ξ and ϕ_η in the diffusion terms represent the derivatives of the dependent variable in ξ and η directions respectively and they can be determined using central differencing scheme such as:

$$\phi_\xi\,|_e=\frac{\phi_E-\phi_P}{\delta\xi} \tag{3.5}$$

$$\phi_\eta\,|_e=\frac{1}{2}\left(\frac{\phi_N-\phi_S}{2\delta\eta}+\frac{\phi_{NE}-\phi_{SE}}{2\delta\eta}\right)=\frac{\phi_N-\phi_S+\phi_{NE}-\phi_{SE}}{4\delta\xi} \tag{3.6}$$

After these arrangements are done for all the other derivatives accordingly and after assigning the value of unity to $\delta\xi$, $\delta\eta$, $\Delta\xi$, $\Delta\eta$ terms from this point on, in order to simplify the calculations,
uation (3.4) becomes:

$$\begin{aligned}&\left(U_f\phi\right)_e-\left(U_f\phi\right)_w+\left(V_f\phi\right)_n-\left(V_f\phi\right)_s=\\&\Gamma_e J^{-1}\alpha\left(\phi_E-\phi_P\right)+\Gamma_e J^{-1}\theta_1\left(\phi_{ne}-\phi_{se}\right)-\Gamma_w J^{-1}\alpha\left(\phi_P-\phi_W\right)-\Gamma_w J^{-1}\theta_1\left(\phi_{nw}-\phi_{sw}\right)\\&+\Gamma_n J^{-1}\theta_1\left(\phi_{ne}-\phi_{nw}\right)+\Gamma_n J^{-1}\beta\left(\phi_N-\phi_P\right)-\Gamma_s J^{-1}\theta_1\left(\phi_{se}-\phi_{sw}\right)-\Gamma_s J^{-1}\beta\left(\phi_P-\phi_S\right)\\&+S_\phi J\end{aligned} \tag{3.7}$$

Defining new variables, equation (3.7) can be expressed in a compact form, such as:

$$\begin{aligned}&C_e\phi_e-C_w\phi_w+C_n\phi_n-C_s\phi_s=\\&D_e\left(\phi_E-\phi_P\right)+S_e\left(\phi_{ne}-\phi_{se}\right)-D_w\left(\phi_P-\phi_W\right)-S_w\left(\phi_{nw}-\phi_{sw}\right)+\\&D_n\left(\phi_N-\phi_P\right)+S_n\left(\phi_{ne}-\phi_{nw}\right)-D_s\left(\phi_P-\phi_S\right)-S_s\left(\phi_{se}-\phi_{sw}\right)+S_\phi J\end{aligned} \tag{3.8}$$

In the equation above, C's represent the convection coefficients, D's represent the diffusion coefficients and S_e, S_w, S_n and Ss represent the additional source terms due to non-orthogonality of the coordinate system. And they are defined as follows in open form:

Convection coefficients:

$$C_e = (\rho J G_1)_e = (U_f)_e \quad \textbf{(3.9a)}$$

$$C_w = (\rho J G_1)_w = (U_f)_w \quad \textbf{(3.9b)}$$

$$C_n = (\rho J G_2)_n = (V_f)_n \quad \textbf{(3.9c)}$$

$$C_s = (\rho J G_2)_s = (V_f)_s \quad \textbf{(3.9d)}$$

Diffusion coefficients:

$$D_e = (\Gamma J^{-1} \alpha)_e \quad \textbf{(3.10a)}$$

$$D_w = (\Gamma J^{-1} \alpha)_w \quad \textbf{(3.10b)}$$

$$D_n = (\Gamma J^{-1} \beta)_n \quad \textbf{(3.10c)}$$

$$D_s = (\Gamma J^{-1} \beta)_s \quad \textbf{(3.10d)}$$

Additional source terms due to non-orthogonality:

$$S_e = (\Gamma J^{-1} \theta_1)_e \quad \textbf{(3.11a)}$$

$$S_w = (\Gamma J^{-1} \theta_1)_w \quad \textbf{(3.11b)}$$

$$S_n = (\Gamma J^{-1} \theta_1)_n \quad \textbf{(3.11c)}$$

$$S_s = (\Gamma J^{-1} \theta_1)_s \quad \textbf{(3.11d)}$$

The dependent variables at the north-east, north-west, south-east and south-west of P, are expressed as the average of the four surrounding nodes as follows:

$$\phi_{ne} = \frac{1}{4}(\phi_P + \phi_E + \phi_N + \phi_{NE}) \quad \textbf{(3.12a)}$$

$$\phi_{se} = \frac{1}{4}(\phi_P + \phi_E + \phi_S + \phi_{SE}) \quad \textbf{(3.12b)}$$

$$\phi_{nw} = \frac{1}{4}\left(\phi_P + \phi_W + \phi_N + \phi_{NW}\right) \quad \textbf{(3.12c)}$$

$$\phi_{sw} = \frac{1}{4}\left(\phi_P + \phi_W + \phi_S + \phi_{SW}\right) \quad \textbf{(3.12d)}$$

Once again, equation (3.8) can be written in a more compact form by grouping all the source terms under one title such as:

$$S_{\phi.t} = S_e\left(\phi_{ne} - \phi_{se}\right) - S_w\left(\phi_{nw} - \phi_{sw}\right) + S_n\left(\phi_{ne} - \phi_{nw}\right) - S_s\left(\phi_{se} - \phi_{sw}\right) + S_\phi J \quad \textbf{(3.13)}$$

and by grouping each cell's dependent variables seperately:

$$C_e\phi_e - C_w\phi_w + C_n\phi_n - C_s\phi_s + \left(D_e - D_w + D_n - D_s\right)\phi_P = D_e\phi_E + D_w\phi_W + D_n\phi_N + D_s\phi_S + S_{\phi.t} \quad \textbf{(3.14)}$$

3.2.1 Discretization of the convection terms

Discretization of the convective terms is of great importance for the accuracy and stability of the numerical computations. The discretization scheme to be used has to have some fundamental properties such as conservativeness, boundedness and transportiveness **(Malalasekera, 1995)**.

The discretization scheme used in this thesis is Hybrid scheme of **Spalding (1972)** based on a combination of central and upwind differencing schemes. A non-dimensional number called the Peclet number is defined as a measure of the relative strengths of convection and diffusion and it is evaluated at the face of the control volume:

$$Pe = \frac{convection\_terms}{diffusion\_terms}$$

for example for an east face:

$$Pe_e = \frac{C_e}{D_e} \quad \textbf{(3.15)}$$

Central differencing scheme, which is accurate to second-order, is employed for small Peclet numbers ($Pe < 2$) and upwind scheme, which is accurate for first order but accounts for the direction of the flow (transportiveness), is employed for large Peclet numbers ($Pe \geq 2$). After the discretization of the convection terms is accomplished, the resulting algebraic equation is:

$$A_P \phi_P = A_E \phi_E + A_W \phi_W + A_N \phi_N + A_S \phi_S + S_{P\phi.t} \qquad \textbf{(3.16)}$$

where

$$A_E = \max(-C_e, \left(D_e - \frac{C_e}{2} \right), 0) \qquad A_W = \max(C_w, \left(D_w + \frac{C_w}{2} \right), 0) \qquad \textbf{(3.17a)}$$

$$A_N = \max(-C_n, \left(D_n - \frac{C_n}{2} \right), 0) \qquad A_S = \max(C_s, \left(D_s + \frac{C_s}{2} \right), 0) \qquad \textbf{(3.17b)}$$

$$A_P = A_E + A_W + A_N + A_S - S_P J \qquad \textbf{(3.17c)}$$

a part of the source term is added to A_P by linearizing it:

$$S_{P\phi.t} = S_{\phi.t} - S_P J \phi_P \qquad \textbf{(3.18)}$$

where S_P must be negative.

4 CONTINUITY AND PRESSURE CORRECTION EQUATIONS

In this chapter, first, the discretization equations for contravariant velocity fluxes U_f and V_f will be derived from the discretization equations for Cartesian velocity components. Then from these equations, with the dependent variables being the contravariant velocity fluxes, the pressure correction equations will be derived. Meanwhile, discretization equation for continuity equation will also be presented. And finally, momentum interpolation method against the problems with pressure-velocity coupling and the occurrence of oscillations in the pressure is given.

4.1 Momentum Equations for Contravariant Velocity Fluxes

If the Cartesian velocity components, *u* and *v* are introduced into eq.(3.16), and pressure term is taken out of the source term, momentum equations are obtained:

$$A_P u_P = A_E u_E + A_W u_W + A_N u_N + A_S u_S - \frac{1}{2} y_\eta (p_E - p_W) + \frac{1}{2} y_\xi (p_N - p_S) + S_{Pu.t} \quad \textbf{(4.1)}$$

$$A_P v_P = A_E v_E + A_W v_W + A_N v_N + A_S v_S + \frac{1}{2} x_\eta (p_E - p_W) - \frac{1}{2} x_\xi (p_N - p_S) + S_{Pv.t} \quad \textbf{(4.2)}$$

Except for the source terms, the corresponding coefficients are identical in these two equations.

Now, the discretization equation for U_f can be obtained by multiplying eq. (4.1) by $(\rho y_\eta)_P$ and eq. (4.2) by $-(\rho x_\eta)_P$ and adding them up. When done so, the resulting equation has velocity components parallel to $(U_f)_P$ on the right side and they are $(U_f^0)_E$, $(U_f^0)_W$, $(U_f^0)_N$ and $(U_f^0)_S$. However this is not a desired result as the two

sides of the equation has got different variables. Therefore, the "actual" neighbors of point P are introduced and the equation gets the following form:

$$A_P(U_f)_P = A_E(U_f)_E + A_W(U_f)_W + A_N(U_f)_N + A_S(U_f)_S$$
$$-\frac{1}{2}\rho\alpha(p_E - p_W) - \frac{1}{2}\rho\theta_1(p_N - p_S) + S_P^U + S_{CURV}^U \qquad \textbf{(4.3)}$$

where:

α and θ_1 are defined before in section 2.1

$$S_P^U = (\rho y_\eta)S_{Pu.t} - (\rho x_\eta)S_{Pv.t} \qquad \textbf{(4.4a)}$$

$$S_{CURV}^U = A_E(U_E^0 - U_E) + A_W(U_W^0 - U_W) + A_N(U_N^0 - U_N) + A_S(U_S^0 - U_S) \qquad \textbf{(4.4b)}$$

↳ represents the curvature effects

and

$$U_E^0 = (\rho y_\eta)_P u_E - (\rho x_\eta)_P v_E \qquad \textbf{(4.5a)}$$

$$U_W^0 = (\rho y_\eta)_P u_W - (\rho x_\eta)_P v_W \qquad \textbf{(4.5b)}$$

$$U_N^0 = (\rho y_\eta)_P u_N - (\rho x_\eta)_P v_N \qquad \textbf{(4.5c)}$$

$$U_S^0 = (\rho y_\eta)_P u_S - (\rho x_\eta)_P v_S \qquad \textbf{(4.5d)}$$

Similarly, the discretization equation for V_f can be obtained by multiplying eq.(4.1) by $-(\rho y_\xi)_P$ and eq.(4.2) by $(\rho x_\xi)_P$

The final resulting discretization equation is:

$$A_P(V_f)_P = A_E(V_f)_E + A_W(V_f)_W + A_N(V_f)_N + A_S(V_f)_S$$
$$-\frac{1}{2}\rho\theta_1(p_E - p_W) - \frac{1}{2}\rho\beta(p_N - p_S) + S_P^V + S_{CURV}^V \qquad \textbf{(4.6)}$$

where

$$S_P^V = (\rho x_\xi) S_{Pv.t} - (\rho y_\xi) S_{Pu.t} \quad \textbf{(4.7a)}$$

$$S_{CURV}^V = A_E (V_E^0 - V_E) + A_W (V_W^0 - V_W) + A_N (V_N^0 - V_N) + A_S (V_S^0 - V_S) \quad \textbf{(4.7b)}$$

and

$$V_E^0 = (\rho x_\xi)_P v_E - (\rho y_\xi)_P u_E \quad \textbf{(4.8a)}$$

$$V_W^0 = (\rho x_\xi)_P v_W - (\rho y_\xi)_P u_W \quad \textbf{(4.8b)}$$

$$V_N^0 = (\rho x_\xi)_P v_N - (\rho y_\xi)_P u_N \quad \textbf{(4.8c)}$$

$$V_S^0 = (\rho x_\xi)_P v_S - (\rho y_\xi)_P u_S \quad \textbf{(4.8d)}$$

Finally, the discretization equation for continuity can be obtained from eq.(3.4) by setting $\phi = 1$ and $S_\phi = 0$:

$$(U_f)_e - (U_f)_w + (V_f)_n - (V_f)_s = 0 \quad \textbf{(4.9)}$$

4.2 Pressure Correction Equation

The need for a correction equation stems from the fact that the velocity field obtained by solving the momentum equations (4.3) and (4.6) do not satisfy the continuity equation. As the starting point of the SIMPLE or SIMPLEC calculation processes, the velocity flux results obtained from the momentum equations are accepted to be the outcomes of a guessed pressure field, *p** and they are represented by U_f^* and V_f^*:

$$A_P (U_f^*)_P = \sum A_{nb} (U_f^*)_{nb} - \frac{1}{2} \rho\alpha (p_E - p_W) - \frac{1}{2} \rho\theta_1 (p_N - p_S) + S_P^U + S_{CURV}^U \quad \textbf{(4.10)}$$

$$A_P (V_f^*)_P = \sum A_{nb} (V_f^*)_{nb} - \frac{1}{2} \rho\theta_1 (p_E - p_W) - \frac{1}{2} \rho\beta (p_N - p_S) + S_P^V + S_{CURV}^V \quad \textbf{(4.11)}$$

where nb stands for the neighboring points of P.

Now, correct values must be defined as the sum of a guessed and a correction part:

$$p = p^* + p' \quad \textbf{(4.12a)}$$

$$u = u^* + u' \quad \textbf{(4.12b)}$$

$$v = v^* + v' \quad \textbf{(4.12c)}$$

Subtracting eq.(4.10) from eq.(4.3) and eq.(4.11) from eq.(4.6), and using the correction formulae (4.12a-4.12c), we obtain:

$$A_P (U'_f)_P = \sum A_{nb} (U'_f)_{nb} - \frac{1}{2}\rho\alpha\left(p'_E - p'_W\right) - \frac{1}{2}\rho\theta_1\left(p'_N - p'_S\right) \quad \textbf{(4.13)}$$

$$A_P (V'_f)_P = \sum A_{nb} (V'_f)_{nb} - \frac{1}{2}\rho\theta_1\left(p'_E - p'_W\right) - \frac{1}{2}\rho\beta\left(p'_N - p'_S\right) \quad \textbf{(4.14)}$$

At this, point, there comes the difference in SIMPLE **(Patankar and Spalding, 1972)** and SIMPLEC **(Van Doormall and Raithby, 1984)** algorithms. In the SIMPLE algorithm, the terms $\sum A_{nb}(U'_f)_{nb}$ and $\sum A_{nb}(V'_f)_{nb}$ are omitted. This is the main approximation of the SIMPLE algorithm and the logic behind is that these terms will be zero when convergence is reached. On the other hand, in the SIMPLEC algorithm, the terms $\sum A_{nb}(U'_f)_P$ and $\sum A_{nb}(V'_f)_P$ are first subtracted from eqns.(4.13) and (4.14), respectively. Then the new terms, $\sum A_{nb}(U'_f)_{nb} - \sum A_{nb}(U'_f)_P$ and $\sum A_{nb}(V'_f)_{nb} - \sum A_{nb}(V'_f)_P$ are dropped from this newly created equation. As these new terms are much smaller than the terms dropped in the SIMPLE algorithm, (U'_f) and (V'_f) are much less affected in the SIMPLEC algorithm. Hence, SIMPLEC algorithm is more reasonable than SIMPLE algorithm.

$$(U_f)_P = (U^*_f)_P + b_P\left(-\frac{1}{2}\rho\alpha\left(p'_E - p'_W\right) - \frac{1}{2}\rho\theta_1\left(p'_N - p'_S\right)\right) \quad \textbf{(4.15)}$$

$$(V_f)_P = (V^*_f)_P + b_P\left(-\frac{1}{2}\rho\theta_1\left(p'_E - p'_W\right) + \frac{1}{2}\rho\beta\left(p'_N - p'_S\right)\right) \quad \textbf{(4.16)}$$

SIMPLE algorithm:

$$b_P = \frac{1}{A_P} \tag{4.17}$$

SIMPLEC algorithm:

$$b_P = \frac{1}{A_P - \sum A_{nb}} \tag{4.18}$$

Yet, in the SIMPLEC, there is the possibility of the denominator to be zero during the iterations. In order to overcome this problem, an underrelaxation factor is used in the discretization equation. So, eq. (3.14) is expressed as:

$$\frac{A_P}{urf}\phi_P = \sum A_{nb}\phi_{nb} + S_{P\phi.t} + (1-urf)\frac{A_P}{urf}\phi_P^{(n-1)} \tag{4.19}$$

here, urf is the underrelaxation factor. $\phi_P^{(n-1)}$ is the value from the previous iteration. With this adjustment, repeating the same procedure b_p for SIMPLEC algorithm can be expressed as follows:

$$b_P = \frac{1}{A_P/urf - \sum A_{nb}} \tag{4.20}$$

Now, the equations (4.15) and (4.16) are to be inserted into the continuity equation. But to avoid solving the pressure correction equation for 9 points (P, N, S, E, W, NE, NW, SE, and SW), the non-orthogonality terms are neglected. Thus, eqns. (4.15) and (4.16) turn into:

$$(U_f)_P = (U^*_f)_P + b_P\left(-\frac{1}{2}\rho\alpha\left(p'_E - p'_W\right)\right) \tag{4.21}$$

$$(V_f)_P = (V^*_f)_P + b_P\left(-\frac{1}{2}\rho\beta\left(p'_N - p'_S\right)\right) \tag{4.22}$$

So now, the equations (4.21) and (4.22) are inserted into the continuity equation, eq.(4.9):

$$(b_P)_e\left[-(\rho\alpha)_e(p'_E - p'_P)\right]-(b_P)_w\left[-(\rho\alpha)_w(p'_P - p'_W)\right]+(b_P)_n\left[-(\rho\beta)_n(p'_N - p'_P)\right]$$
$$-(b_P)_s\left[-(\rho\beta)_s(p'_P - p'_S)\right]+(U^*_f)_e-(U^*_f)_w+(V^*_f)_n-(V^*_f)_s=0$$

(4.23)

rearranging equation (4.23):

$$A_P p'_P = A_E p'_E + A_W p'_W + A_N p'_N + A_S p'_S + m_P \qquad \textbf{(4.24)}$$

where

$$A_E = -(\frac{\rho_P + \rho_E}{2})(\frac{(b_P)_P + (b_P)_E}{2})\alpha_e \qquad \textbf{(4.25a)}$$

$$A_W = -(\frac{\rho_P + \rho_W}{2})(\frac{(b_P)_P + (b_P)_W}{2})\alpha_w \qquad \textbf{(4.25b)}$$

$$A_N = -(\frac{\rho_P + \rho_N}{2})(\frac{(b_P)_P + (b_P)_N}{2})\beta_n \qquad \textbf{(4.25c)}$$

$$A_S = -(\frac{\rho_P + \rho_S}{2})(\frac{(b_P)_P + (b_P)_S}{2})\beta_s \qquad \textbf{(4.25d)}$$

$$A_P = A_E + A_W + A_N + A_S \qquad \textbf{(4.25e)}$$

and

$$m_P = (U^*_f)_e - (U^*_f)_w + (V^*_f)_n - (V^*_f)_s \qquad \textbf{(4.25f)}$$

After the pressure correction equation is solved, velocities are corrected using equations (4.12b) and (4.12c) whereas the pressure is corrected using the equation below:

$$p = p^* + urf_p . p' \qquad \textbf{(4.26)}$$

where urf_p is the underrelaxation factor for pressure.

4.3 Momentum Interpolation Method

As it is the non-staggered arrangement that is being used in this study, the non-physical oscillation or so-called red-black checkerboard splitting of the pressure field problem that was mentioned in the first chapter has to be taken care of. In order to do this, the modified version of **Rhie and Chow (1983)** momentum interpolation method will be used **(Miller and Schmidt, 1988)** to calculate the cell face velocity fluxes.

The discretization equations for U_f and V_f will be used to derive the formulation of the pressure weighted interpolation method (PWIM) or so called momentum interpolation method. Recalling once again eq. (4.3), below will be given the details using U_f only and for V_f, the resulting equation will be given at the end:

$$A_P(U_f)_P = \sum A_{nb}(U_f)_{nb} - \frac{1}{2}\alpha(p_E - p_W) - \frac{1}{2}\theta_1(p_N - p_S) + S_P^U + S_{CURV}^U \qquad \textbf{(4.27)}$$

At this point, the coefficients of the SIMPLE or SIMPLEC algorithm is used and the equation is expressed in an appearance similar to the pressure correction equation, the coefficients, b_P's being defined by eq.(4.17) and (4.20):

$$(U_f)_P = (H_{U_f})_P + (b_P)_P\left(-\frac{1}{2}\alpha(p_E - p_W) - \frac{1}{2}\theta_1(p_N - p_S)\right) \qquad \textbf{(4.28)}$$

where:

$$(H_{U_f})_P = (b_P)_P(\sum A_{nb}(U_f)_{nb} + S_P^U + S_{CURV}^U) \qquad \textbf{(4.29)}$$

However, to simplify things, the cross derivatives of pressure are neglected as in pressure correction equation. Only the influence of ξ-derivatives of pressure on U_f and the η-derivatives on V_f are taken into account. With these considerations, eq.(4.28) becomes:

$$(U_f)_P = (H_{U_f})_P + B_P\left(-\frac{1}{2}(p_E - p_W)\right) \qquad \textbf{(4.30)}$$

where

$$B_P = (b_P)_P \alpha_P \tag{4.31}$$

If equation (4.30) is written for point E (figure 3.2), it gets the following shape:

$$(U_f)_E = (H_{U_f})_E + B_E\left(-\frac{1}{2}(p_{EE} - p_P)\right) \tag{4.32}$$

Now if we use this equation form to express the mainly concentrated term, that is, the velocity flux at the east cell face:

$$(U_f)_e = (H_{U_f})_e + B_e(-(p_E - p_P)) \tag{4.33}$$

At this point, a linearization assumption is introduced to estimate the term, $(H_{U_f})_e$ as follows:

$$(H_{U_f})_e = f^+(H_{U_f})_E + (1 - f^+)(H_{U_f})_P \tag{4.34}$$

where f^+ is the geometric interpolation factor and is defined in terms of the distance between nodal points:

$$f^+ = \overline{Pe}/(\overline{Pe} + \overline{eE}) \tag{4.35}$$

In the equation above, those terms symbolize the distance between those letters (points) and since in the computational domain, those three distances are equal to each other

$f^+ = 1/2$ (for the grid used in this study) **(4.36)**

Now, inserting eq. (4.34) into eq. (4.33) and combining this new equation with eqns. (4.30) and (4.32), we get:

$$(U_f)_e = \frac{1}{2}(U_f)_E + \frac{1}{2}(U_f)_P + B_e\left(-\alpha_e\left(p_E - p_P\right)\right) - \frac{1}{4}B_E\left(-\alpha_E\left(p_{EE} - p_P\right)\right) - \frac{1}{4}B_P\left(-\alpha_P\left(p_E - p_W\right)\right) \quad \textbf{(4.37)}$$

Similarly, the value of (V_f) at the cell face n (north) can be obtained:

$$(V_f)_n = \frac{1}{2}(V_f)_N + \frac{1}{2}(V_f)_P + C_n\left(-\left(p_N - p_P\right)\right) - \frac{1}{4}C_N\left(-\left(p_{NN} - p_P\right)\right) - \frac{1}{4}C_P\left(-\left(p_N - p_S\right)\right) \quad \textbf{(4.38)}$$

where as an illustration,

$$C_P = (b_P)_P \beta_P \quad \textbf{(4.39)}$$

Equations (4.37) and (4.38) are used to evaluate the velocity fluxes at the cell faces. In these equations, if the coefficients, B_E, B_P and C_N, C_P are considered to be approximately equal to B_e and C_n respectively, then equations (4.37) and (4.38) will return back to the expressions of the original Rhie and Chow's scheme.

4.4 Overall Solution Procedure

Now that all the governing equations are examined in detail, it is appropriate to give the procedure of the solution algorithm used in the computer code step by step:

1) Physical properties of the flow and some coefficients defining the solution algorithm like the under relaxation factors are read from an input file.
2) Grid input file prepared in TECPLOT form is read and the grid points are labeled in i, j order.
3) Jacobian and other metric terms of the transformations are computed.
4) Initial conditions of the flow are imposed.
5) Turbulent viscosity, μ_t is computed according to the turbulence model chosen.
6) Contra-variant velocity components are computed at the cell faces using the initialized velocity components.

7) u-momentum discretization equation is solved to obtain the Cartesian velocity component in x-direction.
8) v-momentum discretization equation is solved to obtain the Cartesian velocity component in y-direction.
9) Contra-variant velocity components at the cell faces are updated by using the momentum interpolation method
10) Pressure correction equation is solved
11) Pressure and velocity fields are updated
12) Turbulence kinetic energy equation is solved.
13) Turbulence dissipation rate (or specific dissipation rate if the turbulence model is k-ω) is solved.
14) Turbulent viscosity, μ_t is computed according to the turbulence model chosen.
15) Steps 7-14 are repeated until convergence is reached.

5 VALIDATION CASES

In this chapter, two cases of which experimental datas are available will be used to validate the computer code written for this thesis. Different turbulent models implemented in the code will be compared in performance according to their response in these cases.

The two cases chosen to be used for validation are:

1) Flow through an asymmetric diffuser
2) 2D hill flow

In both cases, there is separation in the flow which is a challenging situation for the computational models. But the first case is a more critical case where the Reynolds number is around 20000 and where it is harder to capture the separation. Conversely, in the second case, the Reynolds number is around 60000 and it is easier to capture the separation.

5.1 Flow Through an Asymmetric Diffuser

This validation case is one of the test cases (test case 8.2) of the 8th ERCOFTAC/IAHR/COST Workshop on Refined Turbulence Modeling, June 17-18, 1999, HUT, Finland. And the results and the experimental datas of this test case are available on the web page:

http://tmdb.ws.tn.tudelft.nl/workshop8/case8_2/case8_2.html

There are three important physical features in this flow, which must be taken into account while handling it numerically: Firstly, there is the fully developed turbulent boundary layer at the inlet with a Reynolds number of 20000 based on the centerline velocity and the channel height. Secondly, there is a smooth-wall separation de to an adverse pressure gradient and prediction of the separation point and the extent of the recirculation region is particularly challenging for computational models. Finally, there is the reattachment and redevelopment of the boundary layer at downstream.

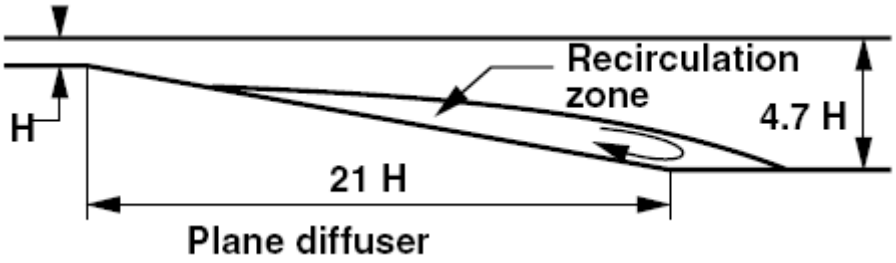

Figure 5.1: Configuration of the Diffuser

5.1.1 Boundary conditions

Inlet

As mentioned above, a fully-developed turbulent velocity profile is used at the inlet (figure 5.2). But the important point here is that the inlet distance, that is, the distance from the inlet to the starting point of the diffuser should be sufficiently long (x/H<-5.87) so that the velocity profile is not affected.

- U is interpolated from the experimental data
- k is computed using the interpolated values of the Reynolds stresses available in the experimental data such as: $k = 1/2\left(\overline{u^2} + \overline{2v^2}\right)$
- ε is computed as , $\varepsilon = C_\mu^{3/4} \dfrac{k^{3/2}}{l}$ for *k*-ε models and ω is computed as,

  $\omega = \dfrac{k^{1/2}}{(\beta^*)^{1/4} l}$ for *k*-ω where $l = -0.07L$ and L is the characteristic length.

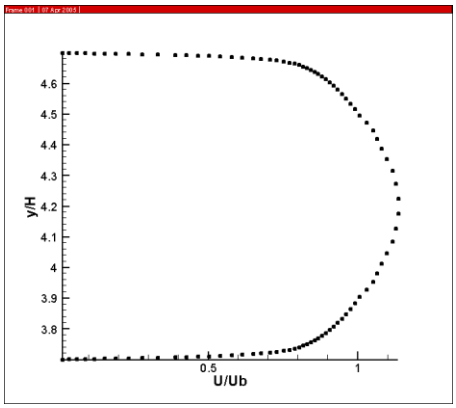

Figure 5.2: Inlet U Velocity Profile for the Asymmetric Diffuser

Outlet

The outlet boundary should be at least at x/H=74 so that one may specify zero-gradient conditions for all the variables.

Upper and Lower Boundaries

The upper and lower boundaries are walls and are treated accordingly in each turbulence model as explained in chapter 2.

5.1.2 Meshes

Two different meshes have been used: fine mesh (265*97) for low Reynolds number k-ε models and k-ω models, coarser mesh (265*53) for k-ε model with wall functions. For the fine mesh, the grid is highly refined close to the walls since the viscous sub-layer has to be solved. Especially for k-ω models, there should be at least 6-7 nodes in the viscous sublayer (y^+<2.5). And for the wall function meshes, the first grid point has to be in the logarithmic layer $30 \le y^+ \le 100$, so the first grid line is placed manually(figure (5.4e)), and then the refinement near the wall is started. Below can be seen the two meshes in several views:

5.1.3 Results

There are 7 test points to be used for validation: 1)x/H=5.98, 2)x/H=13.56, 3)x/H=16.93, 4)x/H=20.32, 5)x/H=27.09, 6)x/H=30.48 and 7)x/H=53.39

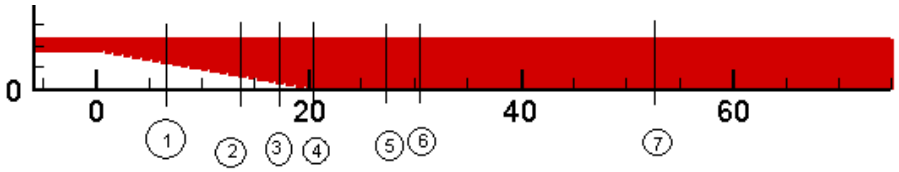

Figure 5.3: Test Points for Asymmetric Diffuser

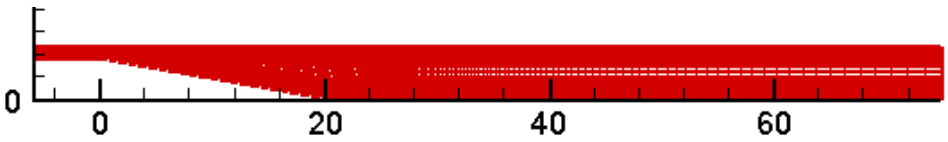

a) Low-Re k-ε and k-ω Mesh

b) k-ε with Wall-Functions Mesh

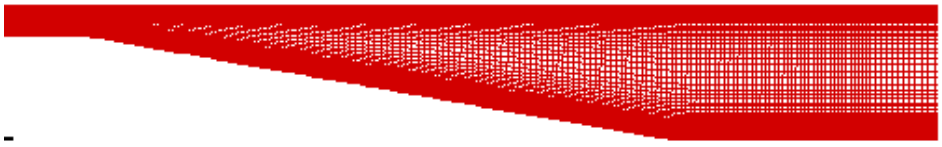

c) Low Re k-ε and k-ω Mesh, Closer Look

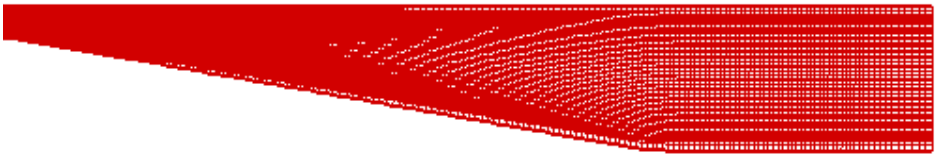

d)) k-ε with Wall-Functions Mesh, Closer Look

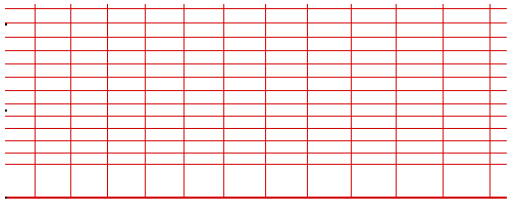

e) k-ε with Wall-Function Mesh, Near Wall

Figure 5.4: Meshes for Asymmetric Diffuser

Here are the mean flow U velocities at the seven test points computed by k-ω88, k-ω98 and k-ε wall-function models and their comparison with the experimental results shown by black dots:

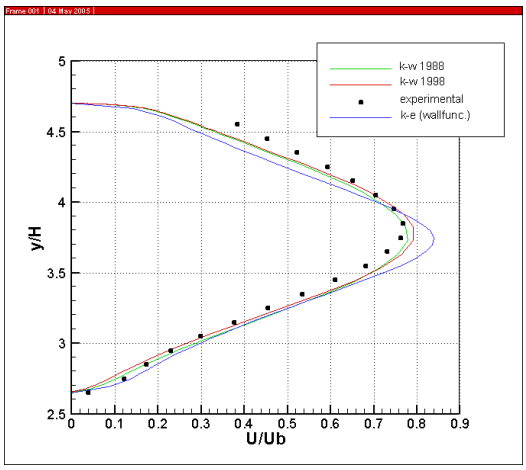

(a) x/H = 5.98

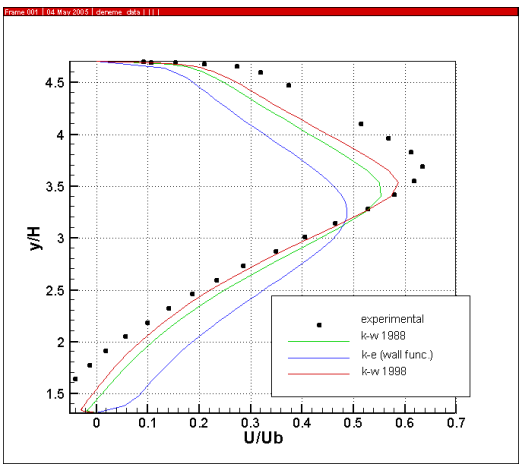

(b) x/H = 13.56

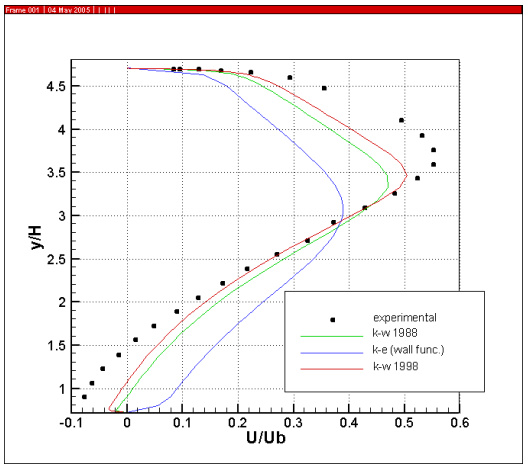

(c) x/H = 16.93

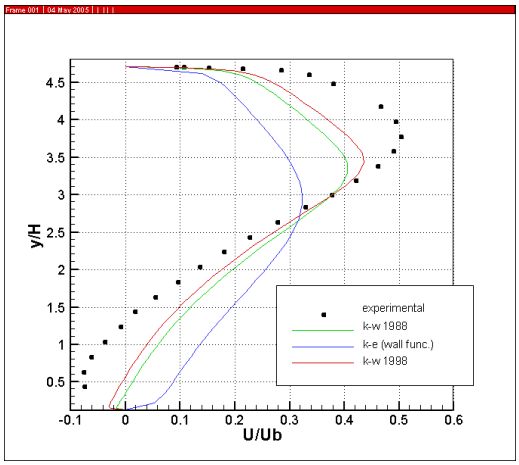

(d) x/H = 20.32

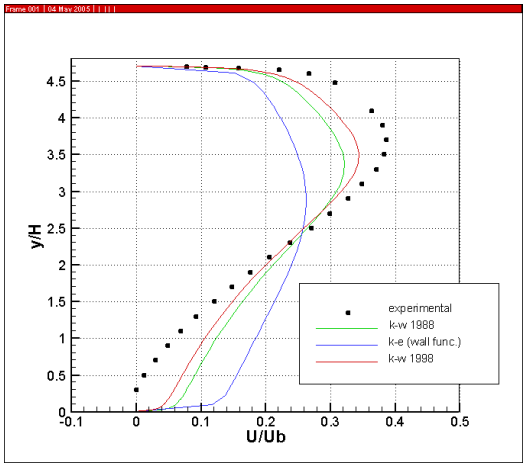

(e) x/H = 27.09

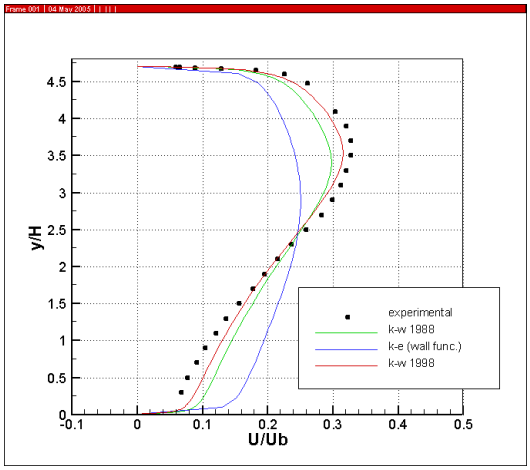

(f) x/H = 30.42

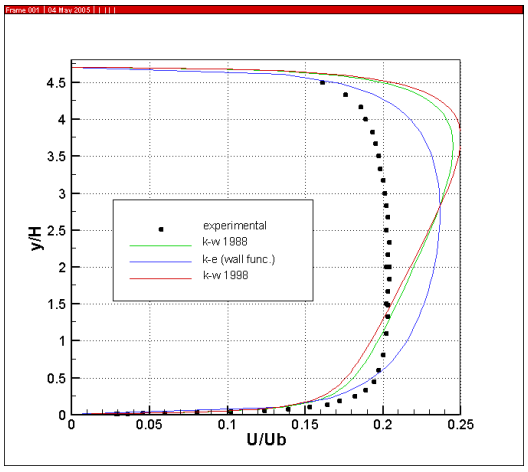

(g) x/H = 53.39

Figure 5.5: Numerical and Experimental Results of U Velocities at Various Positions of the Diffuser

The experimental results are available in dimensionless form by the height of the inlet H and the inlet bulk-velocity U_b. In the numerical computations, H and U_b are both accepted to be equal to 1.

5.1.4 Discussion

Numerical computation was made for 4 different turbulence models presented in chapter 2; namely k-ω models of Wilcox in 1988 and 1998, low Reynolds k-ε model and k-ε model with wall functions. As for the two k-ω models and the low Reynolds number k-ε model, there is viscous sublayer integration in the near wall region which makes the iterating procedure very unstable. Therefore for these three problems all the underrelaxation factors are kept to be very small; around 0.15 and the number of the iterations are very high (70000). But for the k-ε model with wall functions, there is not such a danger of instability. So the underrelaxation factors are higher and the number of iterations is much lower. In figure (5.6) the histories of the iterations can be seen. However, it should be mentioned here that with low Reynolds model of k-ε, the residuals could not be reduced to an acceptable level. So that model's results are not considered here.

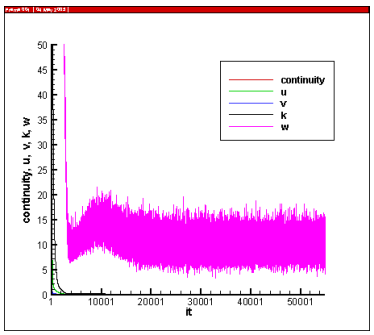

(a) k-ω 1988

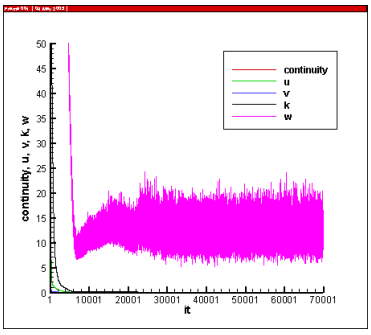

(b) k-ω 1998

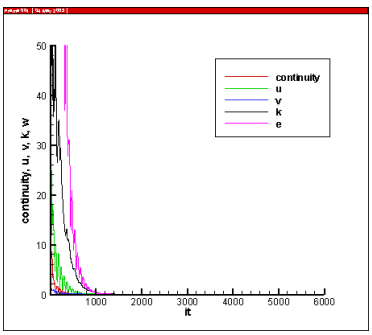

(c) k-ε (wall-func.)

Figure 5.6: Convergence Histories of the Models for Asymmetric Diffuser Problem

In the figure above, it is clearly seen that there are great oscillations in the convergence history of the component, ω. These oscillations show that it is always the dissipation term in the turbulence models that cause the biggest troubles and that are harder to approximate. Now, with these convergence histories in mind, the results can be commented:

- The best results are those of k-ω model 1998. This case is one of the critical examples where it is hard to capture the recirculation region in the flow. k-ε wall function model is not able to capture it anywhere in the flow.

  In the k-ω model 1988 backflow can be realized in very small regions near the wall and the results are still not very good compared to the experimental results. However in k-ω model 1998, results agree with the experiments in the recirculation region.

- Apart from the recirculation region, for example in the 1st and the 7th test points, k-ε model with wall-function agrees not so badly with the experimental results. Especially at the 7th test point where the flow is being fully developed again it is the k-ε model with wall-function that agrees best with the experimental results. And this shows that k-ε model handles the regions away from the wall (free shear regions) better than the k-ω model whereas the k-ω model is far more accurate for boundary layers especially when there is separation.

In appendix A, previous numerical results of this case with the same turbulence models used in this thesis can also be found so as to make a comparison in the numerical performance of the code too. And it is concluded that the numerical results obtained here are completely the same as those previous ones.

5.2 2D Hill Flow

This test case has been presented before at ERCOFTAC Workshop on Data Bases and Testing of Calculation Methods for Turbulent Flows, April 3-7, 1995, University of Karlsruhe, Karlsruhe, Germany (test case 2a, 2D Hill Flow). And the experimental data is available at the web page:
http://cfd.me.umist.ac.uk

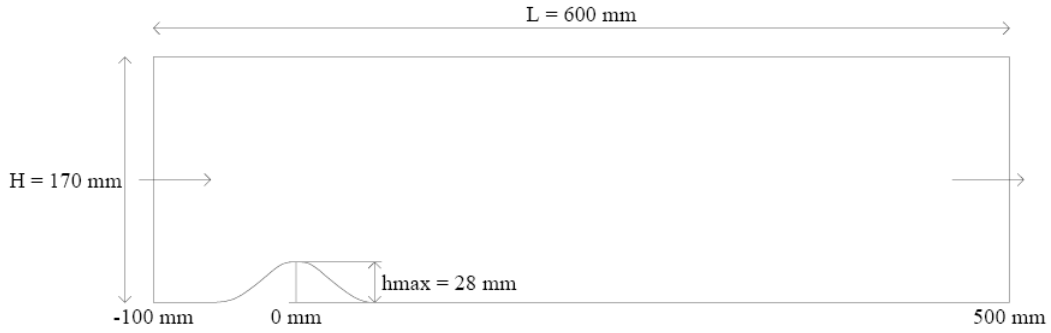

Figure 5.7: Configuration of the Hill

As seen in the figure above, the flow configuration consists of a channel with a hill, located on the bottom of the channel. The most important feature of the flow is that, there is separation after the top of the hill and so a recirculation region. In this second test case, Reynolds number is higher than the first one and it is 60000 based on the centerline mean velocity at inlet, U_0 = 2.147. With the effect of this high Reynolds number, it is not such a critical case as the previous case and it easier for the models to capture the properties of the flow.

5.2.1 Boundary conditions

Inlet

A fully-developed channel flow is used as the inlet boundary condition and it is taken from the experimental data. This time there is both u and v velocity components at the inlet and they are interpolated according to the grid used in the computer code. The methodology to compute the other inlet variables are completely the same as explained in section 5.1.1 except the inlet turbulence kinetic energy. This time, as all the three components of the Reynolds stress are available, it is computed as: $k = 1/2\left(\overline{u^2} + \overline{v^2} + \overline{w^2}\right)$.

Outlet

Fully-developed flow assumption is made and all the gradients are assigned to be zero. But in order to satisfy this assumption, the length of the channel is kept long as advised in the experimental study.

Upper and Lower Boundaries

The upper and lower boundaries are walls and are treated accordingly in each turbulence model as explained in chapter 2.

5.2.2 Meshes

Again two different meshes have been used. The number of nodes in the x-direction is same in both meshes. However, in y-direction, there are more nodes in the meshes for low-Re k-ε model and the two k-ω models (226*161) than for k-ε model with wall functions (229*83). For the nodes in the near wall region, same considerations expressed in section 5.1.2 also hold here.

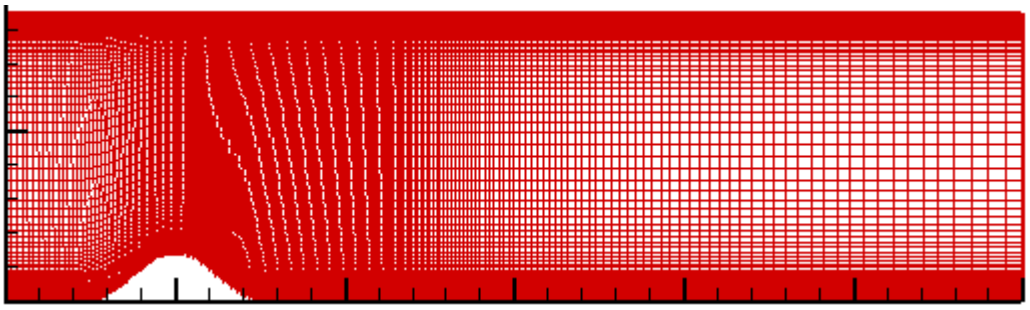

a) low-Re k-ε and k-ω mesh

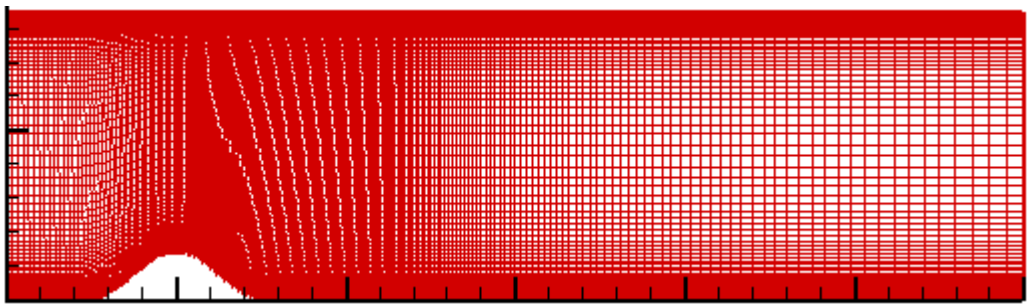

b) k-ε with wall-functions mesh

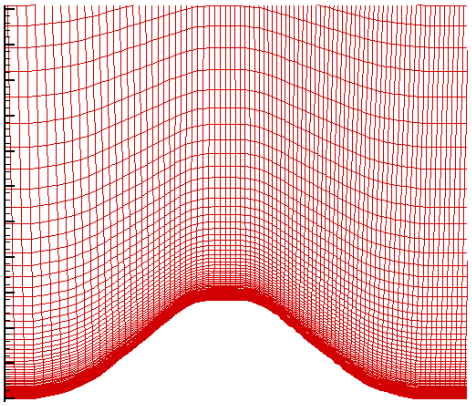

c) low Re k-ε and k-ω mesh, closer look

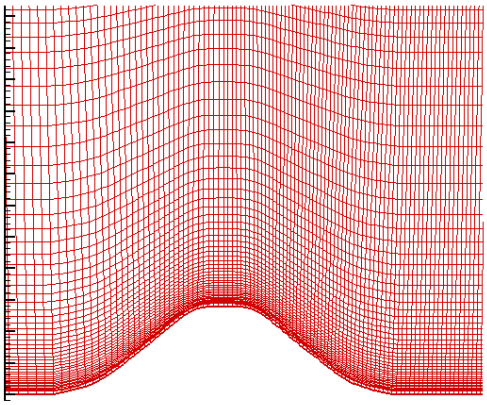

d)) k-ε with wall-functions mesh, closer look

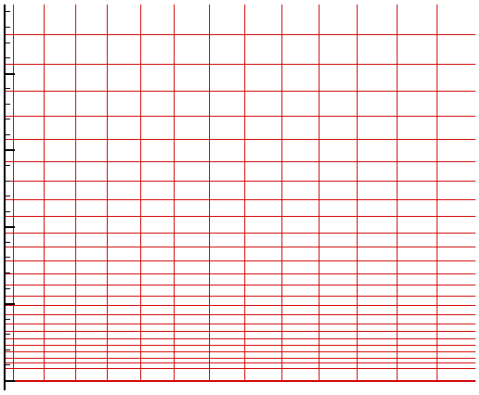

e) k-ε with wall-function mesh, near wall

Figure 5.8: Meshes for 2D Hill

5.2.3 Results

7 test points have been used for validation: 1)x = -50 mm. 2)x = 0 mm. 2)x = 30 mm. 4)x = 50 mm. 5) x = 90 mm 6)x = 134 mm. 7)x = 300 mm.

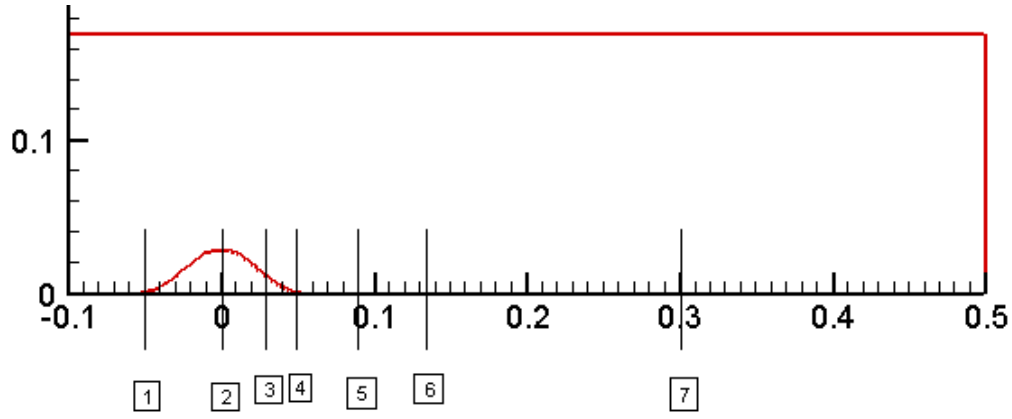

Figure 5.9: Test Points for 2D Hill

Here are the mean flow U velocities at the seven test points computed by k-ω88, k-ω98 and k-ε wall-function models and their comparison with the experimental results shown by black dots:

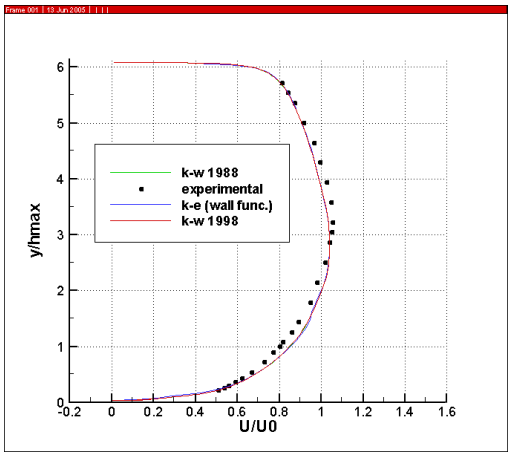

(a) x = -50 mm.

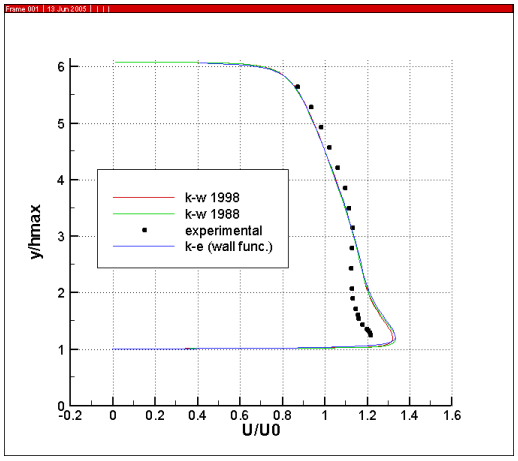

(b) x = 0 mm

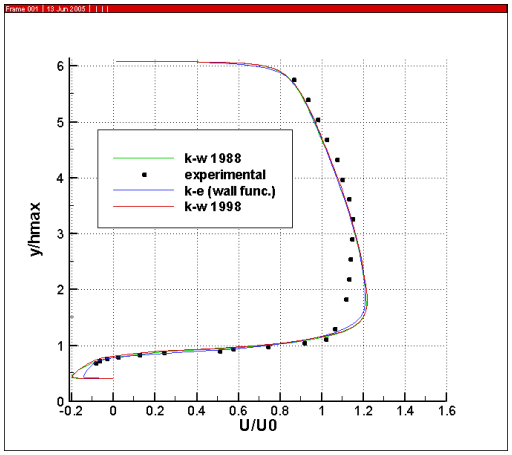

(c) x = 30 mm.

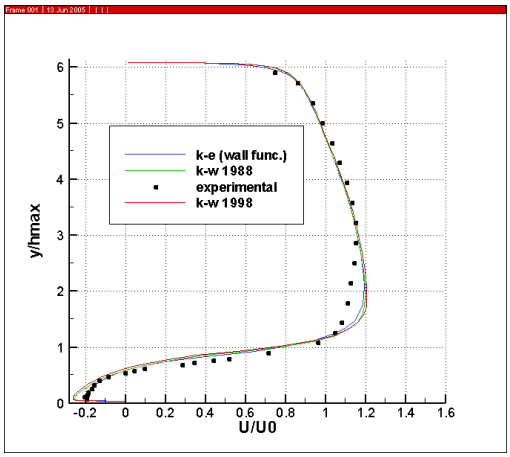

(d) x = 50 mm.

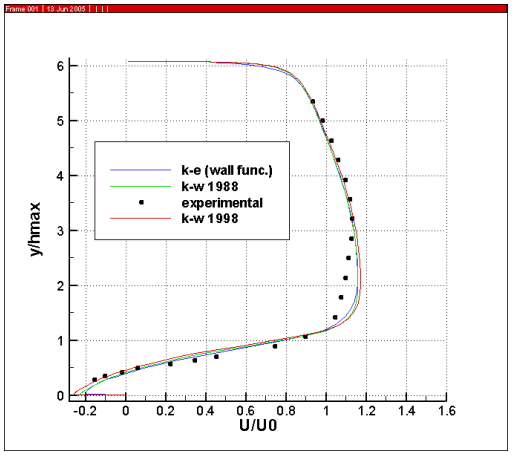

(e) x = 90 mm.

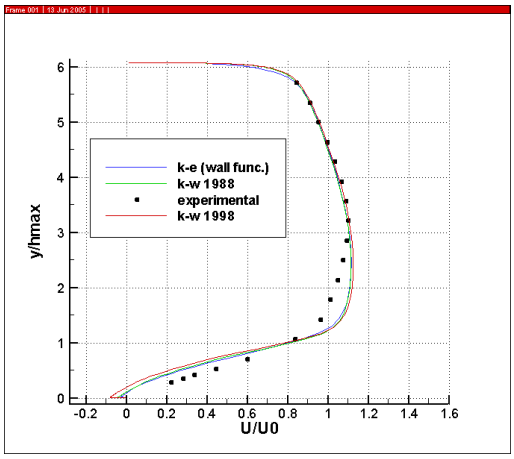

(f) x = 134 mm

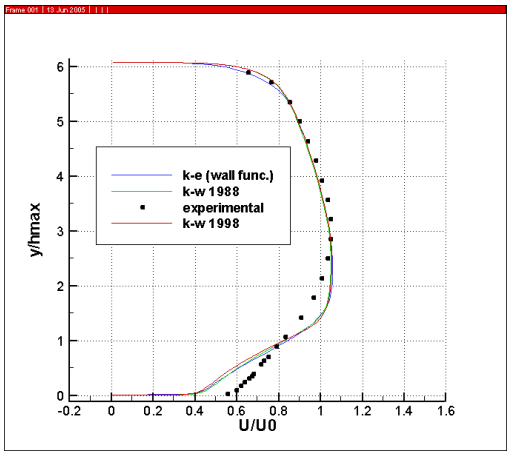

(g) x = 300 mm.

Figure 5.10: Numerical and Experimental Results of U Velocities at Various Positions of the Hill Problem

The experimental results are available in dimensionless form by the height of the hill h_{max} and the mean centerline velocity at the inlet U_0. So results obtained numerically also have been made dimensionless the same way.

5.2.4 Discussion

In this test case again, for the low-RE k-ε model, convergence could not been reached. Therefore, the results for the two k-ω models, k-ω 1988, k-ω 1998 and k-ε model with wall functions will be discussed. The explanation made about the underrelaxation factors and the corresponding iteration numbers are valid here, too.

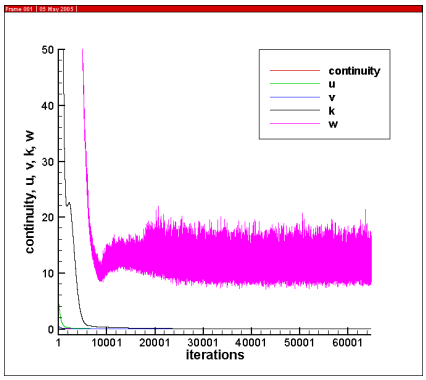

(a) k-ω 1988

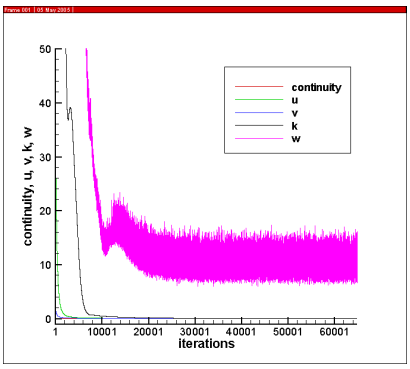

(b) k-ω 1998

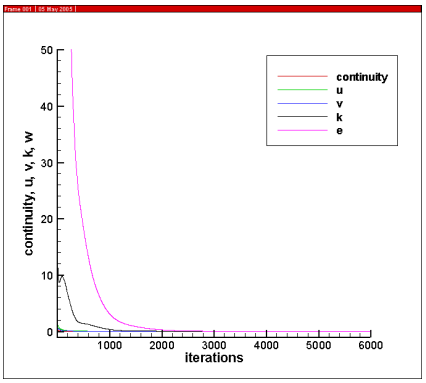

(c) k-ε (wall func.)

Figure 5.11: Convergence Histories of the Models for 2D Hill Problem

Again, as an outcome of the integration through the viscous sublayer and the instability caused by it, big oscillations are observed in the ω, specific dissipation.

The most distinguishing property for this test case when compared with the previous one is that the Reynolds number is very high; 60000. As a result, not only the k-ω models but also k-ε model with wall functions was able to capture the recirculation zone (figure 5.12). Observing only the horizontal velocity components, one cannot see large differences between the models. However, it is the separation point and the reattachment point now that makes the distinction among each model.

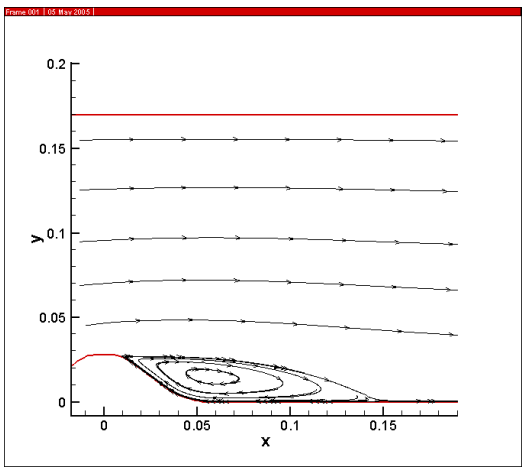

(a) k- ω 1988

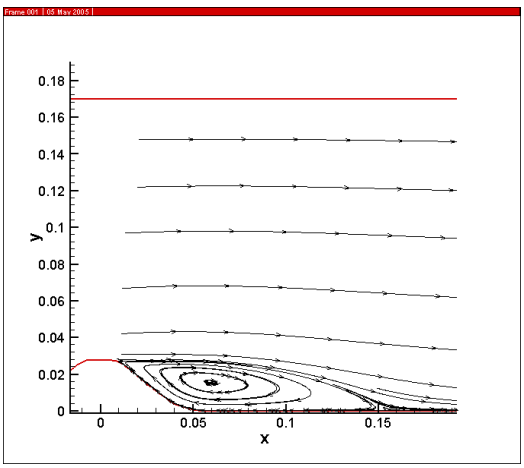

(b) k-ω 1998

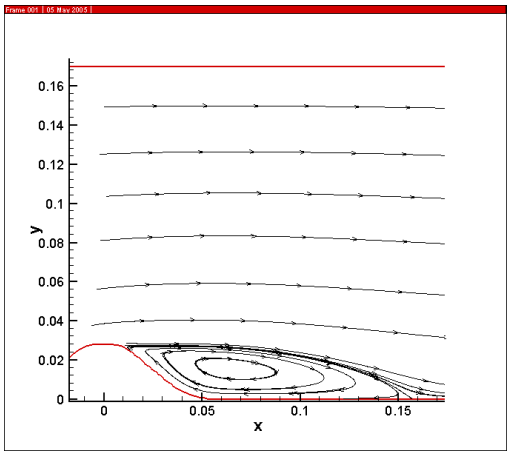

(c) k-ε (wall func.)

Figure 5.12: Streamline Plots of the Recirculation Zone for 2D Hill Problem

If the beginning and the end of the recirculation zone is considered, k-ε model with wall functions gives the best results for the separation point and the reattachment point. Wilcox's k-ω models on the other hand, predict bigger recirculation zones. However if one makes a comparison among them, the 1988 model's results are better. The 1998 model's recirculation zone starts the earliest and ends the latest among all.

Table 5.1: Separation and Reattachment Points Predicted by the Three Models and Obtained by the Experiments

	Separation Point	Reattachment Point
	x(mm)	x (mm)
k-ε (wall func.)	12.26	136.6
k- ω 1988	8.1	151
k- ω 1998	7.67	159
Experiments	12	135

6 CONCLUSION

The main concern of this study is the numerical computation of turbulence flow in complex geometries using a structured grid arrangement and two example cases were handled at the end of the thesis to be able to compare the performance of the computer code written and the turbulence models implemented. The example cases were the flow through an asymmetric diffuser and a 2D hill flow.

Three turbulence models have been implemented successfully: k-ω models of Wilcox that he has developed in 1988 and 1998 and the standard k-ε model with wall functions. Low Reynolds number k-ε model of Lam and Bremhorst is also available in the code but convergence has not been achieved for that model in this study.

The two different cases mentioned above were chosen on purpose in order to illustrate the responses of the turbulence models to different situations. In the first example case, which is the flow through an asymmetric diffuser, Reynolds number is 20000 and this number can be accepted to be a low Reynolds in turbulence flows where the viscous effects are very important especially in the regions close to the wall. Then again, in the 2D hill flow problem, Reynolds number is 60000 and it is accepted to be a high Reynolds number where inertia dominates the flow. As an important thing to mention, there is this common asset in both flows that there is separation and consequently a recirculation region in both which is a challenging condition for computational models.

Regarding this background information, the following conclusions can be made:

- In the diffuser case, the standard k-ε model could not capture the recirculation region at all because the model is unable to solve the viscous effects in the near wall region which is a very important aspect in this specific case.
- In the diffuser case, both of the k-ω models were able to capture the recirculation region. However, with the improvements in the coefficients of dissipation terms in the turbulence equations, the 1998 model gave better results than the 1988 model.

- None of the models was able to predict the redeveloped flow close to the outlet in the diffuser, well. But the standard k-ε model's results were the best qualitatively. It can be said that outside the recirculation region and away from the solid boundaries, its performance is better than the k-ω model.
- In comparison with the diffuser case, in the 2D hill case the viscous effects are not that important as the Reynolds number is very high. Therefore, all the turbulence models capture the recirculation region.
- For the separation point and for the reattachment point in the 2D hill case, standard k-ε model gives the closest results to that of the experiments. And among the two k- ω models, it is the 1988 k-ω model that gives better results. 1998 k-ω predicts the earliest separation point and the latest reattachment point. From this outcome, it can be concluded that in this new version of k-ω, the changes made to take the viscous effects into account, also made the model lose some performance for high Reynolds number flows.

Finally, as a recommendation for further studies:

- The underrelaxation factors have an huge effect on the solution. Therefore one has to be very careful in determining them. Too small underrelaxation factor may lead to too much computation time. On the contrary, if the underrelaxation factor is too big, it may lead the iterations to divergence especially in instable models that consist of viscous sublayer integration.
- Mesh also affects the solution a lot. Particularly, great importance should be given the first node next to the solid boundaries according to the turbulence model used.
- Different turbulence models can be implemented such as k-ω SST, which is a combination of k-ε and k-ω and gives considerably improved results using the advantages of both models in different regions of the flow.

REFERENCES

Basson, A.H., 1992. Numerical Simulation of Steady Three-Dimensional Flows in Axial Turbomachinery Bladerows, *PhD Thesis,* PSU, Pennsylvania.

Boussinesq, J., 1877. Théorie de l'Ecoulement Tourbillant, *Mem. Présentés par Divers Savants Acad. Sci. Inst. Fr.,* **23,** 31-64

Chou, P.Y., 1945. On the Velocity Correlation and the Solution of the Equations of Turbulent Fluctuation, *Quart. Appl. Math.,* **3,** 38.

Daly, B.J. and Harlow, F.H., 1970. Transport Equations in Turbulence, *Physics of Fluids,* **13,** 2634-2649.

Davidov, B.I., 1961. On the Statistical Dynamics of an Incompressible Fluid, *Doklady Akademiya Nauk SSSR,* **136,** 47.

Donaldson, C. duP. and Rosenbaum, H., 1968. Calculation of the Turbulent Shear Flows Through Closure of the Reynolds Equations by Invariant Modeling, *ARAP Report 127,* Aeronautical Research Associates of Princeton, Princeton, NJ.

Harlow, P.H. and Nakayama, P.I., 1968. Transport of Turbulent Energy Decay Rate, Los Alamos Sci. Lab., *University of California Report* LA-3854**.**

Issa, R.I., 1986. Solution of the Implicitly Discretised Fluid Flow Equations by Operator-Splitting, *J. Comput. Phys.,* **62,** 40-65.

Jones, W.P. and Launder, B.E., 1972. The Prediction of Laminarization with a Two-Equation Model of Turbulence, *International Journal of Heat and Mass Transfer,* **15,** 301-314.

Kolmogorov, A.N., 1942. Equations of Turbulent Motion of an Incompressible Fluid, *Izvestia Academy of Sciences, USSR; Physics,* **6,** Nos. 1 and 2, 56-58

Lam, C.K.G. and Bremhorst, K.A., 1981. Modified From of k-ε Model for Predicting Wall Turbulence, *ASME, Journal of Fluids Engineering,* **103,** 456-460.

Launder, B.E. and Spalding D.B., 1972. Mathematical Models of Turbulence, Academic Press, London.

Launder, B.E. and Sharma, B.I., 1974. Application of the Energy Dissipation Model of Turbulence to the Calculation of Flow Near a Spinning Disc, *Letters in Heat and Mass Transfer,* **1(2),** 131-138.

Launder, B.E., Reece, G.J. and Rodi, W. 1975. Progress in the Development of a Reynolds-Stress Turbulence Closure, *Journal of Fluid Mechanics,* **68(3),** 537-566.

Lumley, J.L., 1978. Computational Modeling of Turbulent Flows, *Adv. Appl. Mech.* **18,** 123-176.

Miller, T.F. and Schmidt, F.W., 1988. Use of a Pressure-Weighted Interpolation Method For the Solution of the Incompressible Navier-Stokes Equations on a Non-Staggered Grid System, *Numerical Heat Transfer,* **14(2),** 213-233.

Patankar, S.V. and Spalding, D.B., 1972. A Calculation Procedure for Heat, Mass and Momentum Transfer in Three-dimensional Parabolic Flows, *Int. J. Heat Mass Transfer,* **15,** 1787

Patankar, S.V., 1980 Numerical Heat Transfer and Fluid Flow, Hemisphere Publishing Corporation, Taylor & Francis Group, Newyork

Patel, V.C., Rodi, W. and Scheurer, 1985. Turbulence Models for Near-Wall and Low Reynolds Number Flows: A Review, *AIAA Journal,* **23,** 1308-1319.

Prandtl, L., 1925. Über die ausgebildete Turbulenz, *ZAMM,* **5,** 136-139

Prandtl, L., 1945. Über ein neues Formelsystem für die ausgebildete Turbulenz, *Nacr. Akad. Wiss. Göttingen, Math-Phys. Kl.,* 6-19

Reynolds, O., 1895. On the Dynamical Theory of Incompressible Viscous Fluids and the Determination of the Criterion, *Philosophical Transactions of the Royal Society of London, Series A,* **186,** 123

Reynolds, W.C., 1987. Fundamentals of Turbulence for Turbulence Modeling and Simulation, In Lecture Notes for Von Karman Institute, AGARD Lecture Series No. 86, 1-66, New York : NATO.

Rhie, C.M. and Chow, W.L., 1983. Numerical Study of the Turbulent Flow Past an Airfoil with Trailing Edge Separation, *AIAA Journal,* **21(11)**, 1525-1532.

Rotta, J.C., 1951. Statistische Theorie nichthomogener Turbulenz, *Zeitschrift für Physik,* **129,** 547-572.

Saffman, P.G., 1970. A Model for Inhomogeneous Turbulent Flow, *Proc. R. Soc., Lond.* **A317,** 417-433.

Saffman, P.G. and Wilcox, D.C., 1974. Turbulence-Model Predictions for Turbulent Boundary Layers, *AIAA Journal,* **12(4)**, 541-546.

Shyy, W. and Vu, T.C., 1991. On the Adaptation of Velocity Variable and Grid System for Fluid-Flow Computation in Curvilinear Coordinates, *Journal of Comp. Phys.,* **92(1),** 82-105.

Sondak, D.L. and Pletcher, R.H., 1995. Application of Wall Functions to Generalized Non-orthogonal Curvilinear Coordinate System, *AIAA Journal,* **33,** 33-41.

Spalding, D.B., 1972. A Novel Finite-Difference Formulation for Differential Expressions Involving Both First and Second Derivatives, *Int. J. Numer. Methods Eng.* **4,** 551.

Speziale, C.G., 1985. Modeling the Pressure-Gradient Velocity Correlation of Turbulence, *Physics of Fluids,* **28,** 69-71.

Speziale, C.G., 1987. Second-Order Closure Models for Rotating Turbulent Flows, *Q. Appl. Math.* **45,** 721-733.

Speziale, C.G., 1991. Analytical Methods for the Development of Reynolds Stress Closures in Turbulence, *Annual Review of Fluid Mechanics,* **23,** 107-157.

Van Doormall, J.P. and Raithby, G.D., 1984. Enhancements of the SIMPLE Method for Predicting Incompressible Fluid Flows, *Numerical Heat Transfer,* **7,** 147-163.

Versteeg, H.K. and Malalasekera, W., 1995. An Introduction to Computational Fluid Dynamics: The Finite Volume Method, Harlow, Essex, England : Longman.

Von Karman, T., 1930. Mechanische Ahnlichkeit und Turbulenz, *Proc. Int. Congr. Appl. Mech., 3rd, Stockholm,* Part 1, 85-105

Wilcox, D.C. and Alber, I.E., 1972. A Turbulence Model for High Speed Flows, AIAA Paper, 74-584, Palo Alto, CA.

Wilcox, D.C. and Traci, R.M., 1976. A Complete Model of Turbulence, AIAA Paper 76-351, San Diego, CA.

Wilcox, D.C. and Rubesin, M.W., 1980 Progress in Turbulence Modeling for Complex Flow Fields Including Effects of Compressibility, NASA TP-1517.

Wilcox, D.C., 1988. Reassessment of the Scale Determining Equation for Advanced Turbulence Models, *AIAA Journal,* **26(11),** 1299-1310.

Wilcox, D.C., 1998. Turbulence Modeling for CFD, 2nd Edition, DCW Industries, Inc.

White, F.M., 1974, Viscous Fluid Flow, McGraw Hill, New York.

APPENDIX A

The diffuser problem taken as a test case in this thesis has been solved before by other researchers numerically. The results of those studies using the turbulence models that have been also used in this thesis will be presented here.

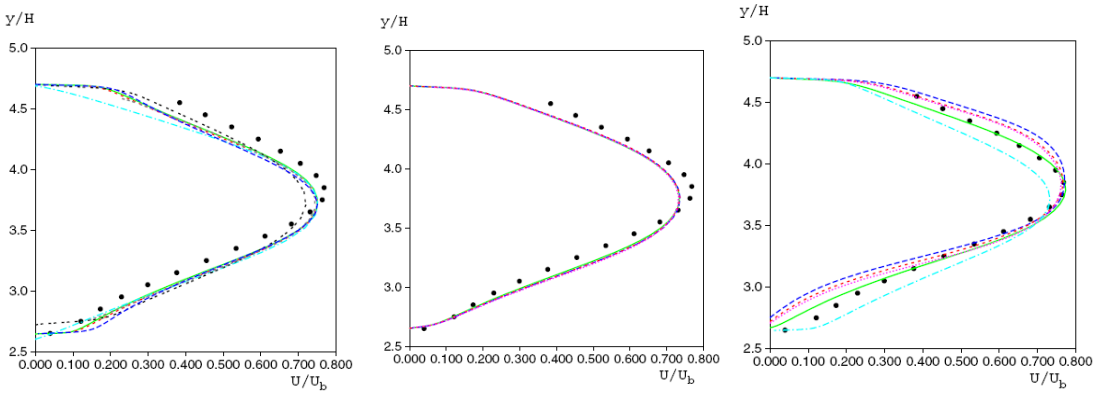

Figure A.1: Previous Numerical Results of U Velocity Profiles of the Diffuser at x /H = 5.98; (a) k-ε, (b) k-ω 1988, (c) k-ω 1998

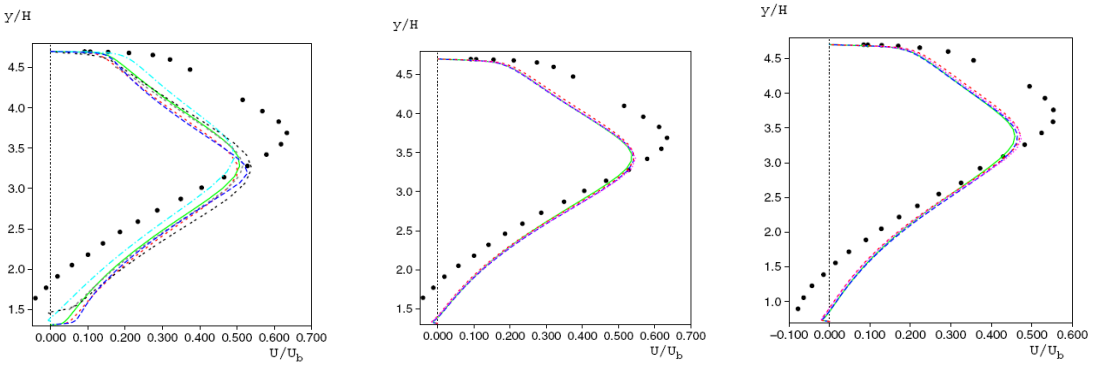

Figure A.2: Previous Numerical Results of U Velocity Profiles of the Diffuser at x /H = 13.56; (a) k-ε, (b) k-ω 1988, (c) k-ω 1998

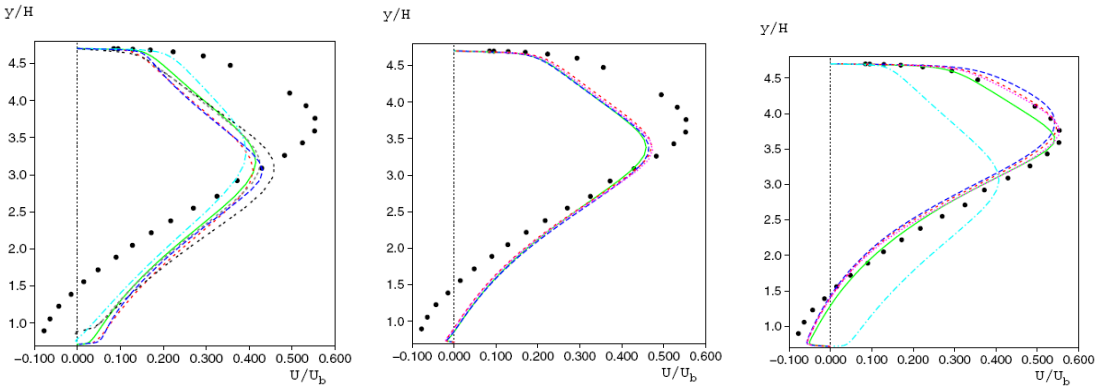

(a) (b) (c)

Figure A.3: Previous Numerical Results of U Velocity Profiles of the Diffuser at x /H = 16.93; (a) k-ε, (b) k-ω 1988, (c) k-ω 1998

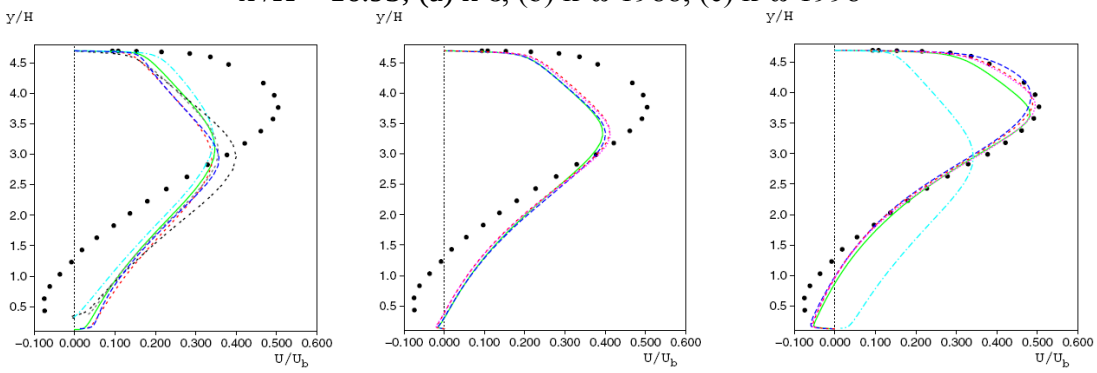

(a) (b) (c)

Figure A.4: Previous Numerical Results of U Velocity Profiles of the Diffuser at x /H = 20.32; (a) k-ε, (b) k-ω 1988, (c) k-ω 1998

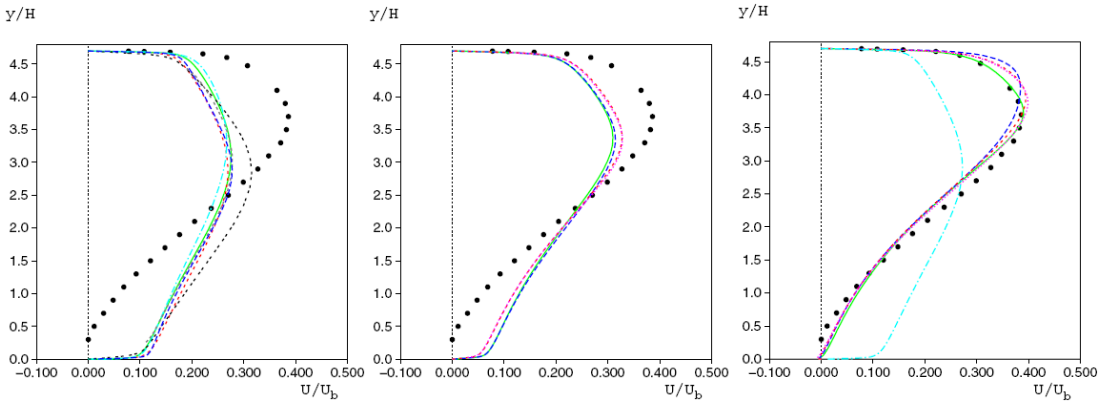

(a) (b) (c)

Figure A.5: Previous Numerical Results of U Velocity Profiles of the Diffuser at x /H = 27.09; (a) k-ε, (b) k-ω 1988, (c) k-ω 1998

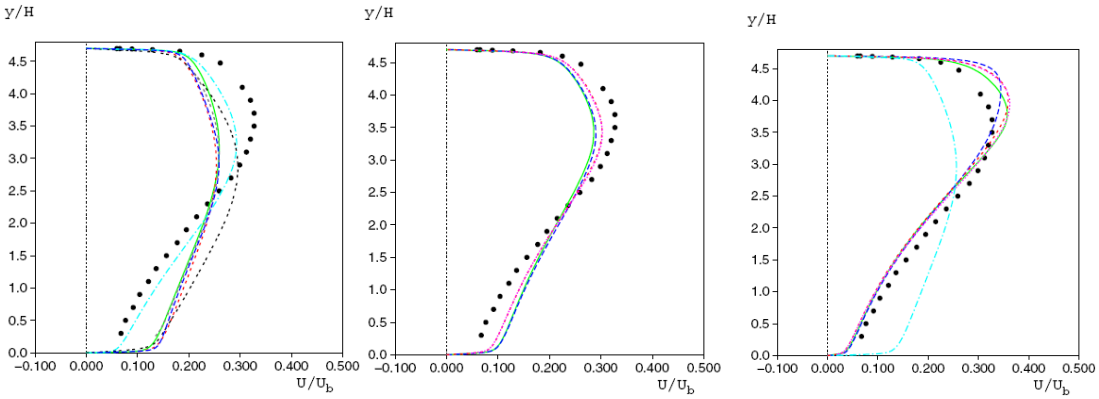

Figure A.6: Previous Numerical Results of U Velocity Profiles of the Diffuser at x /H = 30.48; (a) k-ε, (b) k-ω 1988, (c) k-ω 1998

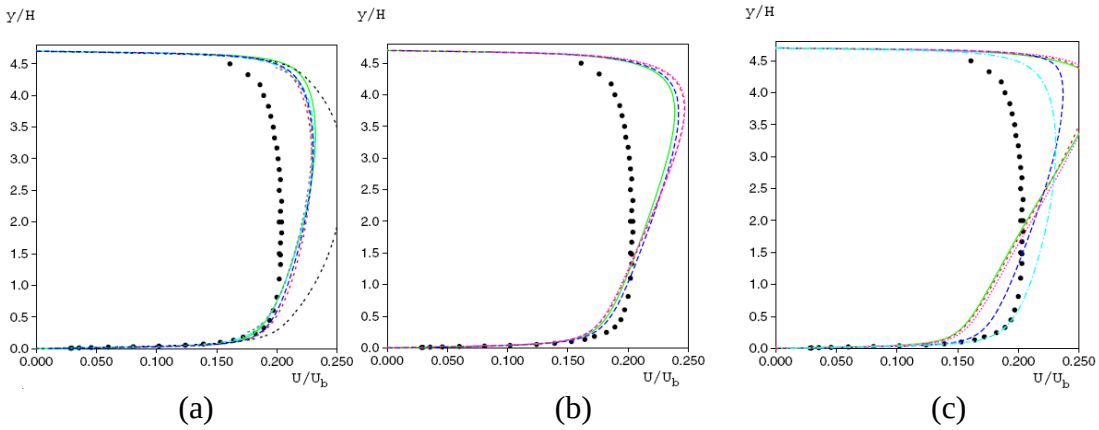

Figure A.7: Previous Numerical Results of U Velocity Profiles of the Diffuser at x /H = 53.39; (a) k-ε, (b) k-ω 1988, (c) k-ω 1998

APPENDIX B

For the test cases used in this study, while deciding upon the number of meshes, the previous numerical studies were used as reference. Yet, those reference numbers were changed slightly sometimes by running the code several times and checking the results. With this kind of studies, it was made certain that the results were free from grid dependency. In the main part of the code, this study was not shown for every single solution. Instead, an example will be given here for one case: the solution of the 2D hill problem with k-ε using wall functions.

This problem was tried using 3 different numbers of meshes: a) 282x103, b) 226x83 and c) 170x63. However as it is very important to locate the first node inside the log layer in this turbulence model, for all the meshes, the first node series above the walls are located manually, and they are the same.

In the end, it was decided that using a 170x63 mesh is enough and it gives the best results (a smaller mesh was tried and it was detected to make the iterations diverge). Below are the results of this grid independency study:

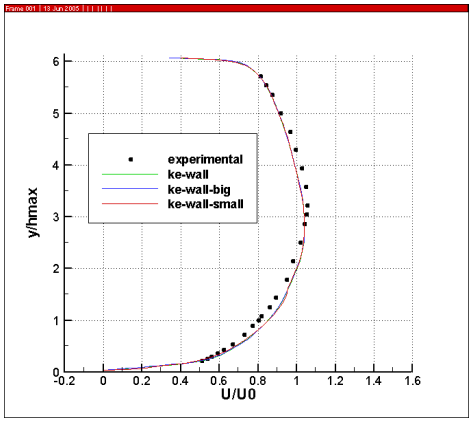

x = -50 mm.

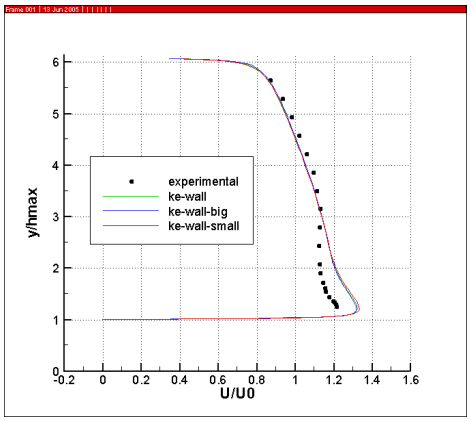

x = 0 mm.

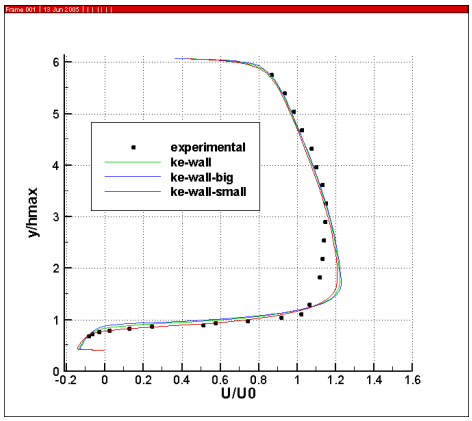

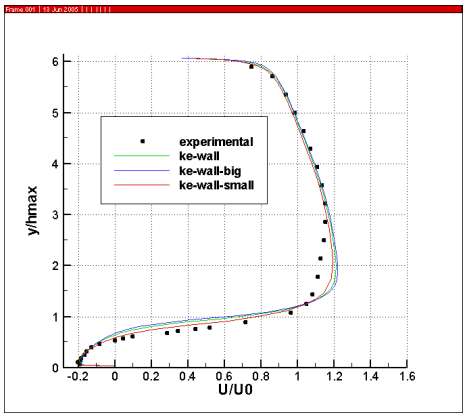

x = 30 mm.

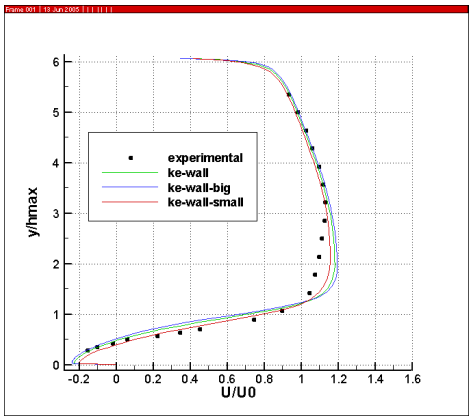

x = 50 mm.

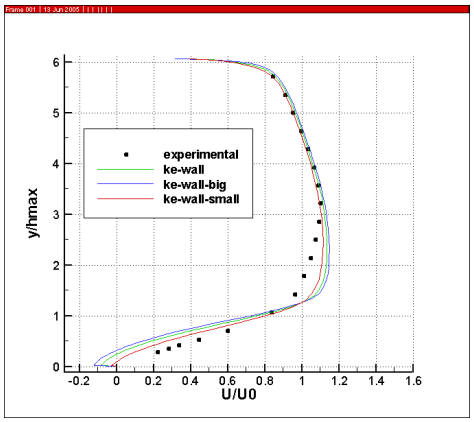

x = 90 mm.

x = 134 mm.

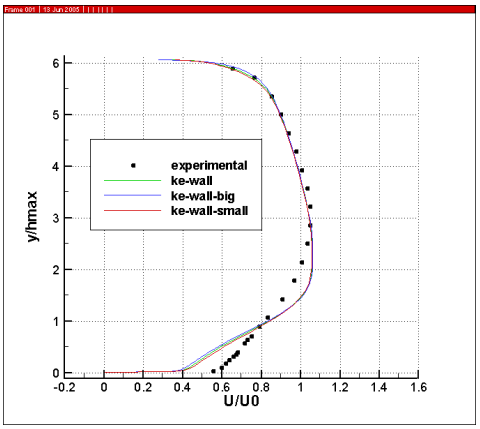

x = 300 mm.

Figure B.1: Grid Dependency Results of the 2D Hill Problem using k-ε Model with Wall Functions

AUTOBIOGRAPHY

Barış Adiloğlu was born in 3rd July 1980. He graduated from Kadıköy Anatolian High School in 1999. In 2001, he got his B.S degree from the Mechanical Engineering Department of Middle East Technical University (METU).